

COLA II - RADIO AND SPECTROSCOPIC DIAGNOSTICS OF NUCLEAR ACTIVITY IN GALAXIES

E. A. CORBETT

Anglo-Australian Observatory, PO Box 296, Epping 1710, NSW, Australia

L. KEWLEY

Harvard-Smithsonian Center for Astrophysics, 60 Garden Street Cambridge, MA 02138

P. N. APPLETON

SIRTF Science Center, MS 220-6, California Institute of Technology, Pasadena, CA 91125

V. CHARMANDARIS¹

Astronomy Department, Cornell University, Ithaca NY 14853

M.A. DOPITA AND C.A. HEISLER²Research School of Astronomy and Astrophysics, Australian National University, Private Bag, Weston Creek
PO, ACT 2611, Australia

R.P. NORRIS

Australia Telescope National Facility, CSIRO, PO BOX 176, Epping NSW, Australia

A. ZEZAS

Harvard-Smithsonian Center for Astrophysics, 60 Garden Street Cambridge, MA 02138

A. MARSTON

SIRTF Science Center, MS 220-6, California Institute of Technology, Pasadena, CA 91125

Draft version October 27, 2018

ABSTRACT

We present optical spectroscopic observations of 93 galaxies taken from the infra-red selected COLA (Compact Objects in Low Power AGN) sample. These are all galaxies for which we have previously obtained low resolution radio observations and high resolution ($< 0.05''$) Long Baseline Array (LBA) snapshots. The sample spans the range of far-IR luminosities from normal galaxies to LIRGs, and contains a significant number of galaxies involved in galaxy-galaxy interactions. Of the galaxies observed, 78 (84%) exhibit emission lines indicating that they are either AGN or actively forming stars (starburst galaxies). Using a newly-developed theoretically-based optical emission-line scheme to classify the spectra, we find 15% of the emission-line galaxies are Seyferts, 77% are starbursts, and the rest are either borderline AGN/starburst or show ambiguous characteristics. We find little evidence for an increase in the fraction of AGN in the sample as a function of far-IR luminosity, in contrast to previous studies, but our sample covers only a small range in infrared luminosity ($10.5 \leq L_{FIR} \leq 11.7$) and thus a weak trend may be masked. Instead, as the infrared luminosity increases so does the fraction of metal-rich starbursts; objects which on more traditional diagnostic diagrams would have been classified as weak LINERs (Low Ionization Narrow Emission Line Regions). As a whole the Seyfert galaxies exhibit a small, but statistically significant, radio excess on the radio-FIR correlation compared to the galaxies classified as starbursts. Compact ($< 0.05''$) radio cores are detected in 55% of the Seyfert galaxies, and these galaxies exhibit a significantly larger radio excess than the Seyfert galaxies in which compact cores were not detected. Our results indicate that there may be two distinct populations of Seyferts, “radio-excess” Seyferts, which exhibit extended radio structures and compact radio cores, and “radio-quiet” Seyferts, in which the majority of the radio emission can be attributed to star-formation in the host galaxy. No significant difference is seen between the IR and optical spectroscopic properties of Seyferts with and without radio cores.

Subject headings: galaxies : active – galaxies : starburst – infrared : galaxies – radio continuum: galaxies

1. INTRODUCTION

Many galaxies exhibit nuclear activity which cannot be directly attributed to stars. Instead, these Active Galactic Nuclei (AGN) are generally believed to be powered by the accretion of matter onto a supermassive black hole (e.g.

Blandford & Rees 1992). Recent kinematic/dynamical studies of nearby galaxies, both with and without AGN, have revealed that many possess a massive central dark object (see e.g. Maoz et al. (1998), Ho (2002), and the review paper by Kormendy & Gebhard (2001)), but it is

¹ Chercheur Associé, Observatoire de Paris, LERMA, 61 Av. de l'Observatoire, F-75014 Paris, France² Deceased

still not known whether all galaxies contain a central black hole. Assuming many, if not all, galaxies possess a massive nuclear black hole, an additional puzzle is that AGNs are only observed in a fraction ($\sim 20\%$) of them.

It is often speculated that the presence of an AGN in a galaxy is in some way related to the circumnuclear environment of the host galaxy. However, although observations have shown that many of the host galaxies of AGN also exhibit circumnuclear phenomena such as starburst activity, inner rings, spirals or bars (e.g. Ho et al. 1997b; Martini & Pogge 1999; Knapen et al. 2000), it is not known whether these signs of activity are related to the mechanisms for fueling an AGN, are triggered by the AGN, or are entirely unrelated to the presence of an AGN. Additionally it has long been speculated that AGN-activity may be triggered and fueled by galaxy-galaxy interactions, yet direct causal links between the degree of interaction and AGN activity have remained elusive, at least at low luminosities (e.g. Bushouse 1986; Keel 1996; Wu et al. 1998; Combes 2001).

Studies of the relationship between AGN and their circumnuclear environment are complicated by the need to quantify the relative strengths of the AGN and any nuclear starburst activity. These measures are often wavelength dependent and can introduce selection biases to the data. An additional problem is the nature of LINERs and their importance in a starburst/AGN regime.

Optical line ratios have long provided a good discriminator between AGN and starburst-dominated galaxies. Galaxies are often classified as AGN or starburst (HII) dominated based on their emission line ratios, following an empirical system developed by Baldwin, Phillips, & Terlevich (1981), and refined by Veilleux & Osterbrock (1987) (hereafter VO87). There are, potentially, situations in which optical spectroscopy may fail to reveal an AGN because of the existence of significant optical obscuration by dust in the galaxy center. This is of particular concern for ultra-luminous infrared galaxies (ULIRGs) and some Seyfert IIs, where large optical and near-IR extinction is suspected (e.g. Genzel et al. 1998; Laurent et al. 2000). However, even in the case of very dusty ULIRGs the optical classification of nuclear activity in all but the most extreme cases is still reliable (Lutz et al. 1998; Genzel et al. 1998; Veilleux et al. 1999; Hwang et al. 1999; Murphy et al. 1999).

Optical line ratios are not the only diagnostic of AGN and starburst emission. The presence of a luminous compact radio core in a galaxy is often taken to be a strong indication of an AGN. Studies such as Norris et al. (1990), Heisler et al. (1998) and Kewley et al. (2000) had a very high detection rate ($\sim 80\text{--}90\%$) of compact cores ($< 0.1''$) in galaxies classified optically as AGN, but compact cores were also detected in galaxies classified optically as starbursts albeit at a considerably lower rate ($\sim 5\text{--}30\%$). In a much higher resolution VLBI study by Smith et al. (1998a, hereafter SLL98), the detection rate of compact cores in AGN and starburst galaxies was found to be similar, with about 50% of the galaxies containing cores. While it is possible that the cores detected in the starburst galaxies could be dust obscured AGN, modeling by SLL98 using estimates of the star formation rate in the host galaxies indicated that many of the lower luminosity compact cores could be explained by emission from complexes of compact

supernovae remnants (RSNe) with a diameter of $\sim 10\text{pc}$. Indeed VLBI observations of Arp 220, a source which was once believed to be powered by a dust-enshrouded AGN, revealed that its core consists of a complex of 12 point sources believed to be RSNe (Smith et al. 1998b). Kewley et al. (2000) found that higher radio-luminosity cores tend to be found in Seyferts rather than starburst galaxies. The radio emission from the high luminosity cores is often more luminous than can be accounted for by synchrotron emission from a single RSNe.

As part of the COLA project, high resolution radio snapshot observations of the southern sample (105) of nearby galaxies were obtained with the Australian Long Baseline Array (LBA) in order to identify compact ($< 0.05''$) high brightness temperature radio cores (Corbett et al. 2002, hereafter Paper I). A study of the northern COLA galaxies is less advanced (P. Appleton et al. in preparation), but is concentrating on the connection between nuclear activity and galaxy-galaxy interactions. In the current paper we present optical spectroscopic observations of 93 galaxies from the southern sample, and use the ratios of the optical emission lines in their nuclear (1 kpc) regions to make spectral classifications. We investigate whether there is any relationship between the properties of the galaxies at radio and infrared wavelengths and their optical classification.

The structure of this paper is as follows: Section 2 contains a brief description of the selection criteria for the galaxy sample and the definitions of quantities used in the paper. The optical spectroscopic observations are presented in Section 3 together with a description of the data reduction and calibration procedure. The optical classifications of the galaxies are discussed in Section 4 and are compared with those obtained for other galaxy surveys. We compare the optical classifications of the galaxies with their infrared, far infrared and radio properties in Section 5 and discuss the relationship between the presence of a compact radio core and galaxy spectral type in Section 6. Finally, in Section 7, we summarize our conclusions. Detailed notes on individual galaxies are included in the Appendix.

2. SAMPLE SELECTION

The COLA galaxy sample consists of an all-sky sample of galaxies in the IRAS Point Source Catalogue (1988) which satisfy the following criteria:

- Flux at $60\mu\text{m}$, $S_{60} > 4\text{Jy}$. If the sources follow the radio-FIR correlation, this flux limit ensures that they have fluxes greater than 10mJy at radio wavelengths and thus the majority ($>90\%$) of the galaxies will be detected at optical - radio wavelengths. The sample was flux limited at $60\mu\text{m}$ as AGN emission is believed to be isotropic at this wavelength (Keel et al. 1994);
- $3500 < \text{helio-velocity} < 7000 \text{ km s}^{-1}$, as measured by Strauss et al. (1992);
- Galactic latitude, $|b|$, greater than 10° to ensure that the IR flux measurements were not contaminated by Galactic cirrus.

The selection criteria and potential sources of bias are discussed in detail in Paper I.

In this paper we use the standard definitions (see e.g. Helou, Soifer & Rowan-Robinson 1985; Sanders & Mirabel 1996) of the infrared flux, S_{IR} , and far-infrared flux S_{FIR}

$$S_{\text{IR}} = 1.8 \times 10^{-14} (13.56S_{12} + 5.26S_{25} + 2.54S_{60} + S_{100}) \text{ W m}^{-2} \quad (1)$$

$$S_{\text{FIR}} = 1.8 \times 10^{-14} (2.54S_{60} + S_{100}) \text{ W m}^{-2} \quad (2)$$

where S_{12} , S_{25} , S_{60} , S_{100} are the IRAS fluxes in Jy of the galaxies at 12, 25, 60 and $100\mu\text{m}$ respectively.

Throughout this paper we assume $H_0 = 75 \text{ km s}^{-1} \text{ Mpc}^{-1}$ and $q_0 = 0.5$ but our conclusions are independent of the exact values adopted. The absolute luminosities quoted in this paper are dependent on both H_0 and q_0 and should therefore be converted if a different cosmology is assumed.

3. OBSERVATIONS

The optical spectroscopic observations were obtained over the period October 1998 - February 2001 with the Dual Beam Spectrograph (DBS) on the 2.3m telescope at the Mount Stromlo and Siding Springs Observatory. Gratings with 1200 lines per mm were used in both the red and the blue arms, giving a resolution of 0.57\AA per pixel and a wavelength coverage of $6000\text{-}7000 \text{\AA}$ and $4600\text{-}5600 \text{\AA}$ in the red and blue arms respectively. A slit width between $1''$ and $2''$ was used during the observations and the spatial resolution is $0.9''$ per pixel. The seeing during these observations varied from sub-arcsecond to more than $2''$, with $1''$ corresponding to between 0.2 and 0.4 kpc at the redshift range of our sample. Three exposures of 300s were initially obtained of each galaxy in our sample, but this was increased to 600s when observing conditions deteriorated. Spectrophotometric and smooth standards (often the same stars) were observed during each night and used to flux calibrate and correct for atmospheric absorption features in the spectra.

Data reduction was carried out in the standard manner using IRAF and a pipeline reduction script. The frames were de-biased (using both bias frames and the bias strip on the individual observations) and flat-fielded. Galaxy spectra were extracted using an aperture centered on the position of peak flux across the slit, and with a width corresponding to 1 kpc (typically 2.5-5 pixels) at the redshift of each galaxy. If more than one peak was seen in the spatial direction, a spectrum was extracted at the position of each peak. Sky-subtraction was then carried out and wavelength calibration done using an Ne-Ar arc lamp. In general an arc lamp observation was obtained immediately after a galaxy observation, i.e. before the telescope was moved to its new position. In a few cases the arc observations were obtained at the end of the night with the DBS rotated to 0, 90, 180 and 270 degrees so as to be within 22.5 degrees of its position during each target observation. This condition allows us to correct for minor wavelength shifts of the arc lines with rotator angle caused by flexure of the spectrograph structure.

The observations were then corrected for atmospheric extinction and flux calibrated using the spectrum of a spectrophotometric standard. Finally the atmospheric absorption features in the target spectra were removed by dividing the spectra by a template atmospheric absorption

spectrum obtained from a smooth spectrum standard observed at a similar airmass to the target. Unfortunately, observing conditions were rarely photometric, and on several nights the seeing was greater than $2.5''$. As a result the flux calibrations are not accurate to better than 30%.

The line fluxes were measured by fitting Gaussians to the emission lines using the *splot* task in IRAF. The continuum flux was subtracted using a linear fit to small portions of the continuum either side of the emission line. The $\text{H}\alpha$ ($\lambda 6562\text{\AA}$) and $[\text{NII}]$ ($\lambda\lambda 6583\text{\AA}, 6548\text{\AA}$) doublet were often blended and their line profiles were de-blended by simultaneously fitting a separate Gaussian for each line. When $\text{H}\beta$ was present in absorption as well as emission both the emission and absorption features were fitted simultaneously with Gaussians. On a few occasions, such as when the emission lines were highly asymmetric, an adequate fit was not obtained by fitting a single Gaussian to each emission line. In these cases, a secondary Gaussian was introduced to each line fit. Generally, this secondary Gaussian had much lower flux than the principal component and a similar FWHM. For the objects treated in this way, the flux measured from the two-component Gaussian fit to each line was summed to give the final flux measured for the line. One galaxy (IRAS 13035-4008) exhibited strong broad $\text{H}\beta$ and $\text{H}\alpha$ components. In this case we attempted to de-blend the broad and narrow components with multi-Gaussian fits and used only the narrow component of the emission lines to calculate the line ratios.

At the upper limit of the redshift range of our sample, the $[\text{SII}]$ doublet ($\lambda\lambda 6730, 6716$) lies in the B-band atmospheric absorption features (at $\sim 6900 \text{\AA}$). It was not always possible to achieve an adequate correction for the absorption features, and so we do not quote the fluxes for the $[\text{SII}]$ emission lines for these objects.

The emission line fluxes measured from the fits to the spectra were corrected for extinction by dust along the line of sight following Veilleux & Osterbrock (1987). The Whitford reddening curve (as parameterized by Miller & Mathews 1972) was used, with the assumption that the ratios of the line intensity at $\text{H}\alpha$ to that at $\text{H}\beta$, is 2.85 for HII-like objects and 3.1 for AGN. Each object was provisionally classified optically as HII region-like or AGN-like (following the procedure described in Section 4.1) before the extinction correction was applied to determine whether the AGN or HII correction was used. For objects lying close to the partition line between the AGN and HII classes, the line fluxes were corrected once assuming an HII-like $I(\text{H}\alpha)/I(\text{H}\beta)$ and once assuming an AGN $I(\text{H}\alpha)/I(\text{H}\beta)$. In practice the extinction correction does not change the spectral classification and thus objects which lie on the partition between AGN and HII are corrected for extinction using the AGN values for the Balmer decrement. The extinction-corrected ratios of the emission lines and the $E(B-V)$ estimates for the COLA galaxies are shown in Table 1.

Optical spectra were obtained for 78 of the 107 galaxies in our initial sample. An additional 15 galaxies in our sample were observed by Kewley et al. (2001b), and since their measurements were obtained using an identical observing and data reduction procedure to our own, we reproduce their results here. The remaining 14 galaxies were not observed due to a combination of poor weather and lack

of telescope time. Aside from ensuring that we obtained optical spectra for those sources in which compact radio cores were detected (see Section 6) the process of deciding which galaxies to observe from the sample of 107 was essentially random. We therefore do not believe that the lack of spectra for a small number of objects will introduce a bias into our results.

We were unable to classify 15/93 galaxies either because $H\beta$ was only detected in absorption rather than emission (6 galaxies) or because no features (either in absorption or emission) were detected in the blue (9 galaxies), probably due to poor signal to noise in the data. In one galaxy, IRAS 10567-4310, $H\beta$ is detected in emission but not [OIII]. An upper limit on the [OIII]/ $H\beta$ ratio has been derived for this galaxy indicating that it is a starburst (or HII) galaxy but we do not plot it on the optical diagnostic diagrams. Ten galaxies exhibit multiple “hotspots”, and the emission line ratios for each hotspot are listed separately in Table 1.

For these observations the slit was positioned by eye over the brightest region of the galaxy and rotated to include any obvious structures or hot spots. It is possible that inaccurate placement of the slit may have resulted in our missing the nucleus in a few cases. Given the small number of objects in which multiple regions of star formation were detected (10/93; 11%) we would expect that inaccurate placement of the slit would be more likely to result in no emission lines being observed (and hence no classification obtained) than an incorrect classification (e.g. a Seyfert galaxy being classified as a starburst galaxy). For this reason galaxies for which we were unable to obtain a classification are excluded from much of the statistical analysis discussed in this paper. There is a possibility, however, that small errors in slit placement may change the line ratios by a small amount. In any case, errors in positioning the slit can only reduce the degree of activity inferred from the line ratios (i.e. denote a Seyfert galaxy to a LINER or a LINER to a starburst galaxy).

4. SPECTRAL CLASSIFICATION

4.1. V95 Classification Scheme

The ratios of the [OIII] $\lambda 5007/H\beta$ lines versus the [NII] $\lambda 6583/H\alpha$, [SII] $\lambda\lambda 6716,6730/H\alpha$, and [OI] $\lambda 6300/H\alpha$ ratios were used to classify the galaxies into starburst (HII region-like) and AGN using the semi-empirical classification scheme developed by VO87.

The galaxies were classified for each diagnostic diagram (Fig. 1) separately and the adopted classification is shown in Table 1. Galaxies which lie below and to the left of the partition line in each diagram are classified as starburst (HII) galaxies. Galaxies which lie above and to the right of the partition line in each diagram are classified as AGN. The AGN-like galaxies were further divided following Veilleux et al. (1995, hereafter V95) into “classic Seyferts” which exhibit high excitation with $[OIII]5007/H\beta \geq 3$ and LINERS which show lower excitation, i.e. $[OIII]5007/H\beta < 3$ (e.g. Heckman et al. 1980). For the remainder of this paper we will use the term V95 to refer to the VO87 classification system with the additional LINER class. In Figure 1, the V95 partition line is shown as a thick dotted line with thin dotted lines at ± 0.05 dex. A thin dotted line is also shown at $[OIII]5007/H\beta = 3$.

AGN with broad Balmer emission lines (i.e. > 2000

kms^{-1}) were classified as Seyfert 1 galaxies. Galaxies which lie within 0.05 dex of the partition line (shown as dotted lines on the diagnostic diagrams; Fig. 1) are classified as borderline or transition objects. The final classification of each galaxy is based on the class given for each diagnostic diagram. Galaxies classified as borderline in at least two diagrams or borderline in one and AGN in another have a final classification of borderline (B). A galaxy classified as HII in two diagrams and borderline in one would have a final classification of HII. Finally, those galaxies which are classified as HII galaxies in one diagram and AGN in another diagram are classified as ambiguous.

For galaxies with multiple “hotspots”, it was necessary to define one overall classification in order to simplify comparison with other surveys and our lower resolution multi-wavelength observations of the galaxies. We have therefore defined the aperture (or “hotspot”) closest to the center of the galaxy as the “nuclear” spectrum and it is this classification which is used for the galaxy in the analysis described in Sections 5 and 6. On one occasion it was impossible to determine which hotspot was the more central and the hotspot with the brightest emission lines was designated the “nuclear” spectrum. The additional “hotspots” detected represent secondary emission line regions (generally fainter than those of the “nuclear” hotspot), possibly due to a galaxy merger, and may even be additional nuclei. It can be seen from Table 2 that the majority (10/13) of these additional emission line regions are classified as starbursts, with the remaining three classified as ambiguous (2) or borderline starburst (1).

According to the V95 classification scheme, we find that 12 of the galaxies in our sample are Seyferts and 45 are dominated by starburst emission (Table 2). Excluding the 15 galaxies for which no spectral classification was obtained, this amounts to 15.4% Seyferts and 57.1% starburst with the remainder having borderline (10.2%), LINER (7.7%) or ambiguous (9.0%) classifications, in good agreement with other similar studies. For example, from observations of 182 luminous infrared galaxies ($L_{\text{IR}} > 3 \times 10^{10} L\odot$) V95 classified 59% as starbursts and 14% as Seyferts. Similarly, Kewley et al. (2001a; hereafter K01), using the same system as V95, classified 58% of galaxies as starbursts and 18% as Seyferts from a sample of 225 galaxies selected on the basis of their IR colour ($8 > S_{60}/S_{25} > 0.5$ and $2 > S_{60}/S_{100} > 0.5$) and flux ($S_{60} > 2.5 \text{ Jy}$). A series of papers by Ho et al. (1997a) (hereafter H97), investigates the prevalence of low luminosity AGN (so called “dwarf” Seyfert galaxies) from spectroscopic observations of 486 nearby ($z \sim 0$) galaxies. Of the galaxies with emission line nuclei they classify $\sim 12\%$ as Seyferts and $\sim 50\%$ as starburst galaxies.

4.2. K01 Classification Scheme

Recently, K01 used detailed stellar population synthesis and photoionization models to develop an alternative scheme for the classification of starburst and AGN. This scheme is based on the standard emission line diagnostic diagrams and new theoretical classification lines. K01 demonstrated that their new theoretical scheme reduces the number of ambiguous classifications when compared to the V95 scheme, concluding that the position of the theoretical lines are more consistent from diagram to dia-

gram than the semi-empirical V95 method. We also used this scheme to classify the COLA galaxies. The theoretical lines are shown as thick solid lines in Figure 1, with thinner solid lines at ± 0.5 dex. As before, galaxies are classified as starbursts if they lie below and to the left of the theoretical line, and as AGN if they lie above and to the right of the theoretical line. As with the V95 system, galaxies which lie within 0.5 dex of the line are classed as borderline (B). Galaxies which fall within the AGN region on one or two diagrams and the starburst region on the remaining diagram(s) have been given “ambiguous” classifications.

Using the K01 diagnostic diagrams results in a higher fraction of the galaxies being classified as starburst galaxies (76.9%) than from the V95 diagrams (Table 2). This is at the expense of the LINER, borderline and ambiguous classes which fall to 0%, 2.6% and 5.1% of the galaxy classifications respectively. All the galaxies classified as AGN were also classified as Seyferts under the V95 system and will therefore be referred to as Seyferts for the remainder of this paper. The fact that the number of ambiguous classifications as a whole is lower for the K01 scheme (4/93; 5%) than the V95 scheme (7/93; 9%) supports the conclusion by K01 that their theoretical scheme produces more consistent classifications from diagram to diagram. It is also interesting to note that all six galaxies classified as LINERs under the VO87 system are reclassified under the K01 system (3 as starburst galaxies, 2 as ambiguous and 1 as borderline). A more detailed investigation of the galaxies which change classification under the different schemes is given in an companion paper (P. Appleton et al., in preparation) but one possibility is that the original V95 “LINER” classification actually encompasses AGN/starburst composites and metal-rich starbursts, the latter resulting in low $[\text{OIII}]/\text{H}\beta$ ratios but high $[\text{NII}]/\text{H}\alpha$ ratios.

4.3. AGN Contribution

The theoretical models developed by K01 have been used recently to develop mixing grids which allow the contribution of an AGN to the optical emission-line ratios to be found (Kewley et al. 2002, hereafter K02). Since there exists a range of possible starburst-AGN ratios due to the various combinations of ionization parameter and metallicity possible, K02 defined a maximum and a minimum mixing grid for each diagnostic diagram, which give the largest possible range in the AGN-related contribution to the optical emission-line ratios. The AGN contribution was calculated for each diagnostic diagram using the average result from the maximum and minimum mixing grids. The final AGN contribution used is an average from the three diagnostic diagrams, and is given in Table 3. The lower and upper limits on the AGN contribution for each galaxy are given by the lowest and highest contributions found out of all three diagrams.

It is important to note that this AGN contribution is an estimate of the amount of AGN contribution to the optical emission line ratios *only* (eg. $[\text{OIII}]/\text{H}\beta$, $[\text{NII}]/\text{H}\alpha$, $[\text{SII}]/\text{H}\alpha$, and $[\text{OI}]/\text{H}\beta$), not an estimate of the AGN contribution to the continuum, luminosity, or to the emission-lines by themselves. Nevertheless, the AGN contribution

can serve as a useful indicator of the relative amount of star formation and AGN activity responsible for the radiation which ionizes the narrow emission-line gas. The 12 galaxies classified as Seyferts using both the V95 and K01 schemes are marked with an astrix (*) in Table 3. It is interesting to note that out of these 12 Seyfert galaxies, 4 have optical AGN contributions under 50%, and one galaxy (IRAS 03022-1232) has an AGN contribution of only 25% to the total emission. The fact that an AGN needs to contribute only a small proportion of the emission line ratios for the galaxy to be classified as an AGN was also noted by K01, and is most likely due to the log-log nature of the diagnostic diagrams, making them particularly sensitive to the presence of an AGN, even when dominated by star formation. Massive star formation is generally expected near the nuclei of infrared luminous galaxies since interactions with companions, formation of bars, and other instabilities can efficiently drive large amounts of gas to the center (see Bryant & Scoville 1999; Combes 2001).

Compact nuclear starbursts and AGN in IR galaxies may be enshrouded by large quantities of dust (Clavel et al. 2000). In these cases, the emission is optically thick in the optical and near-IR, and the spectral energy distribution peaks in the far-IR (40–100 μm). As a result, even if the presence of an AGN is revealed in the optical, it is difficult to quantify the effect of dust absorption and the reprocessing of its energy to longer wavelengths. To measure the AGN contribution to the bolometric luminosity of active galaxies better, diagnostics in mid-IR wavelengths, where we are less affected by extinction, have been developed (see Lutz et al. 1998; Genzel et al. 1998; Laurent et al. 2000; Charmandaris et al. 2002a, and references therein). Recent results using such IR diagnostics suggest that most ultraluminous infrared galaxies dominated by star formation in the optical are also dominated by their star formation in the infrared (Genzel et al. 1998; Lutz et al. 1999). However, while observations in the mid-IR can probe the dusty cores of IR bright galaxies much better than visible observations, the cores can still be optically thick in the mid-infrared. Furthermore, only a small fraction ($\sim 3\text{--}5\%$) of the total luminosity of the most luminous infrared galaxies emerges in the mid-IR (Charmandaris et al. 2002b)³. Ideally one would want to directly probe the physical properties of the nucleus in wavelengths where most of the energy of those galaxies appears, but unfortunately the spatial resolution at far-IR is rather poor.

5. INFRARED AND RADIO PROPERTIES

5.1. Infrared Properties

The IR fluxes used to select the original sample (see also Corbett et al. 2002) were taken from the *IRAS Point Source Catalogue* (Beichman et al. 1988). However, these fluxes are believed to be less accurate than those given in the *Faint Source Catalogue (FSC)* (Moshir et al. 1990). These new FSC fluxes are used for the analysis of the COLA galaxies, and are shown in Table 4.

It has long been proposed that the spectral class is linked with infrared luminosity (L_{IR}). In general, AGN are found in galaxies which exhibit higher L_{IR} than starburst galaxies selected from the same volume-limited sample (e.g.

³ For normal late type galaxies it has been shown that $\sim 15\%$ of the luminosity is emitted between 5–20 μm (Dale et al. 2001)

Sanders88; V95). To investigate such a dependency in the COLA sample, we split our sample into a number of luminosity ranges (shown in Fig. 2a; Table 5). Using the K01 classification scheme, we find that the proportion of starburst and Seyfert galaxies in each luminosity bin remains roughly constant with luminosity. In fact the Student t-Test reveals no statistical difference between the infrared luminosity of the Seyfert galaxies and the starburst galaxies. The number of galaxies with an ambiguous classification increases from $\sim 0\%$ (0/22) with $L_{\text{IR}} < 10^{10.75}$ to $\sim 18\%$ (2/11) with $L_{\text{IR}} > 10^{11.25}$ but the small number of ambiguous galaxies in our sample (5/93) means that this trend is probably not significant.

Veilleux et al. (1999, hereafter V99) conducted an optical spectroscopic study of 108 ultraluminous infrared galaxies ($L_{\text{IR}} > 10^{12}L_{\odot}$) and combined it with V95 ($L_{\text{IR}} > 3 \times 10^{10} L_{\odot}$). They found that the proportion of galaxies classified as AGN (Seyferts and LINERS) increased with IR luminosity, contrary to our findings.

One possible explanation for this discrepancy is that the V99 sample extends into the ULIRG regime ($L_{\text{IR}} > 10^{12}$) whereas our sample contains only 11 objects with $L_{\text{IR}} > 10^{11.25}$. Our sample may simply not cover a large enough range in luminosity to identify a weak trend or, alternatively, the onset of a larger fraction of AGN may depend on a threshold effect around $10^{12}L_{\odot}$ (see also Tran et al. 2001). On the other hand, it may be that the different classification schemes (V99 used the V95 scheme) are responsible for the discrepancy. We therefore re-examined the data using the V95 classifications and found that the proportion of starburst galaxies did indeed decrease with IR luminosity, falling from $\sim 60\%$ at $L_{\text{IR}} < 10^{10.75}L_{\odot}$ to $\sim 45\%$ at $L_{\text{IR}} > 10^{11.25}L_{\odot}$ (Table 5, Fig. 2b). No obvious trend with luminosity was seen in the Seyferts but the proportion of LINERS, borderline and ambiguous galaxies rose from 14% ($L_{\text{IR}} < 10^{11}L_{\odot}$) to 36% ($L_{\text{IR}} > 10^{11.25}$). A Student t-Test indicates that the mean L_{IR} of the combined LINER, borderline and ambiguous galaxies is higher than that of the V95 classified HII galaxies with a probability of $< 1\%$ of being due to chance. Note that 21 galaxies are classified as LINERS, ambiguous or borderline galaxies under the V95 system, whereas the majority of these galaxies (15/21) are reclassified as starburst galaxies under the K01 system.

It has long been known (e.g. de Grijp et al. 1985) that Seyferts exhibit warmer IR colors, as measured by the ratio of emission at $60\mu\text{m}$ to that at $25\mu\text{m}$. Consequently, AGN candidates have often been selected on the basis of warm IR colors (e.g. de Grijp et al. 1985, K01). We find that Seyferts make up 20% (9/43) of the galaxies with $S_{60}/S_{25} < 8$ (the selection criterion used in K01 to select AGN candidates) and only 6% (3/50) galaxies with $S_{60}/S_{25} > 8$ with a probability of $< 2\%$ of such a distribution being obtained by chance, in good agreement with previous studies. The warm FIR colors exhibited by AGN are believed to be due to the hot gas and dust in the torus which is heated by emission from the accretion disk (Pier & Krolik 1993; Efstathiou & Rowan-Robinson 1995). Using the K01 classification scheme we find that there is no significant difference between the proportion of starburst

galaxies with $S_{60}/S_{25} < 8$ (70%, 30/43) and $S_{60}/S_{25} > 8$ (60%, 30/50). The majority (14/15) of galaxies for which we were unable to measure line ratios have $S_{60}/S_{25} > 8$, confirming our suspicion that these galaxies do not possess an excess of hot dust and are not active, hence the lack of measurable $\text{H}\beta$ emission.

The galaxies classified as LINERS, borderline and ambiguous using the V95 system tend to have cool FIR colors (14/21 have $S_{60}/S_{25} > 8$) with a statistical probability $< 0.1\%$ that the difference between their mean FIR colour compared to that of the starburst galaxies is due to chance. By contrast we find that the galaxies classified as borderline using the K01 system tend to have warm FIR colors (2/2 have $S_{60}/S_{25} < 8$) while those with an ambiguous classification tend to have cooler FIR colors (3/4 have $S_{60}/S_{25} > 8$) and starburst-like [NII] and [SII] line strengths with unusually strong [OI] emission⁴. The small number of borderline and ambiguous galaxies from the K01 system means that it is not possible to determine whether these trends are significant.

Our results imply that for galaxies with $L_{\text{IR}} < 10^{12}L_{\odot}$ there is no evidence that the fraction of Seyfert galaxies increases with L_{IR} . However, there is some evidence that the proportion of galaxies classified as LINERs, borderline and ambiguous galaxies using the V95 classification system does increase with L_{IR} . These galaxies are reclassified as starburst/ambiguous galaxies, using the K01 system, and the fact that they tend to have cool FIR colors, unlike the Seyfert galaxies, supports the view that they are “unusual” (metal-rich) starbursts rather than AGN. One interpretation of this is that as L_{IR} approaches $10^{12}L_{\odot}$ starburst galaxies migrate into the metal-rich starburst region of the K01 diagrams, where they would become classified as LINERs/ ambiguous in the more traditional diagnostic diagrams (thus skewing the statistics away from starbursts). This will be investigated further in Appleton et al.

5.2. Radio-FIR Properties versus Galaxy Classification

The total integrated radio luminosities of the Southern COLA galaxies at 4.8, 2.5 and 1.4GHz were published in Paper I together with the results of Australian LBA snapshot observations. At 4.8GHz, 104 of the 107 galaxies were detected at the 5σ level. A summary of the radio measurements is given in Table 4.

Three galaxies (IRAS 05449-0651, IRAS 10484-0153 and IRAS 15555-6610) were not detected at 4.8GHz. IRAS 10484-0153 is classified as a starburst galaxy and has a 60 micron flux of 4.51 Jy so should have been detected at radio wavelengths if it was to follow the radio-FIR correlation. The other two galaxies are predicted to be weak at radio wavelengths based on their far-IR fluxes. IRAS 05449-0651 and IRAS 15555-6610 were originally included in the COLA sample as their $60\mu\text{m}$ fluxes were listed as greater than 4 Jy in the *IRAS Point Source Catalogue*, but their fluxes in the *Faint Source Catalogue* fall well below 4 Jy (0.85 and 2.41 Jy respectively). These three galaxies have been excluded from the analysis which follows.

A tight correlation was seen between the radio and FIR luminosity of the southern COLA galaxies (Fig. 2; Paper I). This correlation is well-known and is seen across

⁴ Curiously the one ambiguous galaxy which exhibits warm IR colors (IRAS 00085-1223) also exhibits strong (AGN-like) [NII] emission, possibly indicating that it is a composite galaxy.

many different galaxy magnitudes and types (Helou, Soifer & Rowan-Robinson 1985; Sanders & Mirabel 1985; Yun & Hibbard 2001). It is often attributed to star formation in the disk of the galaxies: the FIR emission produced by dust heated by young stars and the radio emission from electrons accelerated in supernovae. Following Helou, Soifer & Rowan-Robinson (1985), we define the parameter $q = \text{Log}(S_{\text{FIR}}/S_{\text{radio}})$ to quantify the relative strengths of the radio-FIR emission, where S_{radio} is the total radio flux of the galaxy at 4.8GHz. Table 6 shows the mean, median and standard deviation, σ , of q for the different galaxy types as classified using the K01 classification scheme. The median q for the whole Southern COLA galaxies is 2.80 ± 0.03 . The 59 starburst galaxies (excluding IRAS 10484-0153 which was not detected at radio wavelengths) in our sample exhibit a tight radio-FIR correlation with a median $q = 2.83$ (mean $q=2.81$), and a relatively small scatter ($\sigma=0.2$). The Seyfert galaxies (11 galaxies as IRAS 15555-6610 is now excluded) exhibit a much larger scatter ($\sigma=0.49$) and a significantly smaller median q of 2.55 (mean $q=2.41$), indicating that the Seyfert galaxies exhibit a radio excess on the radio-FIR correlation. The Student t-Test indicates that the difference in mean q between the two samples is significant with a probability $<10^{-5}$ of being a chance occurrence. Since q is related to the radio and FIR luminosity of the galaxies and we found no correlation between the FIR luminosity and the spectral classification of the galaxies (section 5.1), we expect to find some correlation between radio luminosity and spectral classification. A Student t-Test on the data reveals that this is indeed the case as galaxies classified as Seyferts have a group average radio luminosity higher than that of starbursts, with a probability $P=1.7 \times 10^{-4}$ of such a distribution being due to chance. Note, however, that the correlation of spectral type with q is much stronger than that with radio luminosity.

The galaxies with ambiguous or borderline classifications exhibit similar values of q to the starburst galaxies (mean $q=2.78 \pm 0.05$ and 2.83 ± 0.05 respectively). This result suggests that the radio emission in these galaxies is dominated by star formation-related processes, confirming the result of Roy et al. (1998).

6. COMPACT CORES VERSUS SPECTRAL CLASSIFICATION

High resolution, single baseline snapshots were obtained with the Australian LBA of 105/107 of the galaxies in the Southern COLA sample. The remaining two galaxies, of which only one is included in the sub-sample discussed in this paper (IRAS 05053-0805), were not observed due to technical difficulties. These observations, described in greater detail in Paper I, were conducted at 2.3GHz and would detect radio emission $\geq 1.5\text{mJy}$ from structures $\leq 0.5''$ in size, corresponding to brightness temperatures $> 10^5\text{K}$. Since we did not obtain LBA observations of IRAS 05053-0805 it has been excluded from the analysis which follows.

Compact radio cores were detected in 9/105 ($\sim 9\%$) objects observed and the detected fluxes (and upper limits for the non-detections) are given in Table 4. The cores detected ranged in luminosity from $L=10^{3.5-5.0}\text{L}_\odot$ (7 have $L>10^4\text{L}_\odot$) while the median upper limit for non-detections is $L=10^{3.78}\text{L}_\odot$ with only 6 sources having upper limits on

their core luminosity $> 10^4$. The COLA galaxy sample was constrained to lie within a thin shell of redshift space in order to reduce any distance dependent biases. The range exhibited in detection upper limits owed as much to differences the sensitivities of the telescopes used in the course of these observations as to the spread of distances of the objects in our sample.

Six of the eleven galaxies (55%) in which we detect compact radio cores are classified optically as Seyfert galaxies while only three were detected in the 59 galaxies classified as starburst by the K01 system. The positions of the galaxies with compact cores on the optical diagnostic diagrams are shown in Fig. 3 (filled symbols) from which we can see that two of the three starburst galaxies (IRAS 09375-6951 and IRAS 13097-1531) are actually classified as borderline objects using the V95 system.

To determine whether the detection rates of compact cores in Seyferts and starburst galaxies were significantly different, we performed the following statistical analysis, assuming a binomial distribution with the detection/non-detection of a compact core as the success/failure criterion. Mindful of any biases due to e.g. different detection limits for sources, we used only those sources in which cores were detected with $L>10^4\text{L}_\odot$ or in the case of non-detections, upper limits of $L<10^4\text{L}_\odot$. This resulted in the elimination of 2 of the 9 sources in which compact cores were detected (one Seyfert and one starburst galaxy) and 6 of the galaxies without compact cores (4 starburst galaxies and 2 with ambiguous classifications). We further restricted our analysis to include only those galaxies for which we have obtained a spectral classification. The resultant sample contained 10 Seyferts, 53 starburst galaxies and 4 ambiguous or borderline objects. Initially the detection rate of compact cores in starburst galaxies was used to estimate the probability of detecting a compact core in a given source (2/53) assuming all galaxies have the same probability of containing a compact core, irrespective of spectral type. We found that the probability of detecting 5 cores in a sample 10 objects is $P = 1.4 \times 10^{-5}$, indicating that the detection rate of cores in Seyferts is indeed significantly higher than that in starburst galaxies. Of course, the actual detection rate may be underestimated by using the starburst detection rate so our calculations were repeated for a detection rate of 7/67 (i.e. that of cores $L>10^4\text{L}_\odot$ in all galaxies with a spectral classification). This time the probability of detecting 5 cores in a subset of 10 objects rose to 0.0018 (still less than 0.5%) while the probability of detecting only two cores out of a subset of 53 galaxies became highly unlikely ($P<10^{-5}$). It is therefore clear that Seyferts and starburst galaxies exhibit statistically different detection rates for compact radio cores.

The Seyfert galaxies with compact cores display a significant radio excess (median $q=2.27$) relative to the starburst galaxies without compact cores (Fig. 4) with a probability $< 10^{-8}$ (from the Student t-Test) that this excess is due to chance. Again these galaxies also have higher radio luminosities than the starburst galaxies (median radio power $=3.8 \times 10^{22} \text{ W Hz}^{-1}$ and $6.6 \times 10^{21} \text{ W Hz}^{-1}$ respectively), but the significance of this ($P \sim 10^{-7}$) is slightly smaller than for q . By contrast, the Seyfert galaxies without compact cores exhibit q values and radio luminosities which are not significantly different from those displayed

by the galaxies optically classified as starburst galaxies (median radio power = 5.5×10^{21} W Hz $^{-1}$, median $q = 2.79$; Table 6). These results imply that the source of the radio emission in the Seyfert galaxies without cores is the same as that of the starburst galaxies - i.e. star formation in the galactic disk (e.g. Kennicutt 1998) - in good agreement with Roy et al. (1998). The AGN itself must contribute little to the overall radio emission in this scenario. The alternative explanation that the radio and FIR emission from the AGN without compact cores are related and scale in a similar manner as the radio and FIR emission from star formation seems somewhat improbable.

The radio emission from the radio cores detected in the Seyfert galaxies is too weak to account for their low q values, and in Paper I we concluded that the most probable explanation is that they exhibit a radio excess due to extended structures (at the ~ 100 pc - 1 kpc scale) associated with the radio cores, e.g. small-scale jets and/or radio lobes. Indeed one of the objects in which a compact radio core is detected (IRAS 13197-1627) does display an extended linear structure ~ 280 pc in length (Kinney et al. 2000).

Although we cannot rule out the presence of a compact radio core in the non-LBA detected Seyfert galaxies we can place an upper limit of $L < 10^{3.7}L_\odot$ on any such core. Only one of the Seyferts in which we detect a compact core (IRAS 12329-3938) has a core luminosity $L < 10^4L_\odot$ and while this source also exhibits the lowest FIR luminosity and second lowest radio luminosity of all the Seyferts (including those not detected with the LBA) it still exhibits a significant radio excess ($q=2.5$). The non-detection of compact cores and lack of a significant radio excess in the 5 Seyferts without cores therefore implies that not only must their radio cores (if present) be intrinsically weaker relative to their host galaxy than those in the Seyferts with cores but also that these objects lack extended radio structures.

The previous statement should not be taken to mean that the Seyfert galaxies without compact cores are “weak” AGN. From the estimated AGN contributions to the optical line ratios presented in Table 3, there is no evidence to suggest that the Seyferts with compact cores exhibit larger AGN contributions to the optical line ratios than those without (Fig. 3). Similarly, Student t-Tests on the data indicate that there are no statistically significant differences between the mean IR luminosity and colors of the Seyferts with compact cores and those without. In fact we argue that it is only at radio wavelengths that two Seyfert populations emerge; “radio excess” Seyferts, which exhibit compact radio cores and an excess of radio emission relative to their FIR luminosity, and “radio-quiet” Seyferts in which the vast majority of radio emission can be attributed to star formation in the host galaxy.

Compact cores are also detected in three galaxies classified as starbursts by the K01 system. In the Seyfert galaxies, the significant radio excess we observe suggests that their compact cores are associated with a radio jet but the origin of the compact radio emission in the starburst galaxies is not so obvious. While the presence of a high-brightness-temperature compact radio core is usually evidence of an AGN, the situation is much less certain for lower luminosity compact cores.

Significant differences do exist between previous studies of compact cores in starburst galaxies. In the South, Norris et al. (1990) detected compact ($< 0.1''$) radio cores at 2.3 GHz in only 5% of their starburst galaxies and 32% of AGNs with $L_{\text{FIR}} > 10^{10}L_\odot$. With the same spatial resolution and sensitivity (> 5 mJy) as the Norris et al. survey, Heisler et al. (1998) detected no compact cores in their starburst galaxies and a much larger fraction (90%) of the AGN in their survey of $60\mu\text{m}$ peakers. Kewley et al. (2000) found a larger fraction ($\sim 37\%$) of starbursts and a similar fraction (80%) of AGN-type galaxies with compact ($< 0.1''$) cores. Some of these differences may be due to differing sensitivity limits, or to the different ways in which the parent samples were selected. The majority of the Kewley et al. starbursts have core fluxes < 5 mJy and would not have been detected in the Norris et al. and Heisler et al. surveys. As mentioned in the introduction, SLL98 also carried out a VLBI study in the north and found little difference in detection rate (53 – 54%) between optically classified AGN and starbursts (see also Lonsdale et al. 1993). The SLL98 observations generally have a higher resolution than the southern observations, and their sample contains galaxies with higher luminosities ($L_{\text{FIR}} > 10^{11.25}L_\odot$) – both factors that could account for the different statistics. In all the surveys, the authors were unable to rule out a SNRe origin for the low luminosity compact radio emission detected in starburst galaxies.

Our results confirm that compact cores tend to be more prevalent in galaxies with Seyfert classifications (6/11) than starburst galaxies (3/58). Of the three starburst galaxies, two of them, IRAS 13097-1531 and IRAS 09375-6951, have core radio luminosities $L > 10^4L_\odot$, which has been taken by Kewley et al. (2000) to indicate a likely AGN rather than a SNR origin. Despite the fact that these galaxies have cool IRAS colors (see earlier discussion), they also exhibit a slight excess in the radio-FIR correlation.

Notes on the individual Seyfert galaxies in our sample and the starburst galaxies in which compact cores were detected are given in the Appendix.

7. CONCLUSIONS

We present optical spectroscopic observations of 93 galaxies selected from the southern portion of the COLA survey. The spectra have been used to classify the galaxies into various types based on the strength of key emission lines using both traditional semi-empirical (V95) and a new theoretically predicted (K01) diagnostic ratios. These spectroscopic diagnostics of nuclear activity are compared with other probes, such as IRAS colors and the existence of a compact radio core as a measure of activity. The following conclusions are reached:

- For the COLA (south) sample, we find that the fraction of Seyfert galaxies in the sample is independent of the diagnostic method used (16%), but that the fraction of starburst systems does depend on the choice of diagnostic. Using the V95 method, we find $\sim 57\%$ are starbursts, 8% are LINERs and 19% are ambiguous or borderline, whereas under the K01 system, 77% are classified as starbursts, none are classified as LINERs and a smaller fraction (8%) fall into the ambiguous or borderline category. This

is a result of model predictions which suggest that metal-rich starbursts can have emission-line ratios which place them into the phase-space occupied by LINERs in the semi-empirical diagnostic diagrams.

- The COLA sample covers only the far-IR luminosity range of normal galaxies to Luminous Infrared Galaxies (LIRGs) and falls short of sampling the ULIRG region ($L_{\text{IR}} > 10^{12} L_{\odot}$). Using the K01 classification system, our spectra suggest little change in the fraction of Seyfert galaxies relative to starbursts as a function of far-IR luminosity – in contrast to previous work. We note, however, that the narrow range of luminosities covered by our sample may not allow us to identify a weak trend in our data. Our result suggests either that there is a threshold IR luminosity above which AGNs begin to dominate the population, or that, as the galaxies become more IR luminous, there is a tendency for them to migrate into the metal-rich starburst region of the K01 diagrams, where they would become classified as LINERs in the more traditional diagnostic diagrams (thus skewing the statistics away from starbursts). We note that the COLA sample contains a high fraction of interacting systems which are known to be metal-rich in their nuclei; such a migration would be consistent with galaxies becoming IR luminous as they evolved through collisions.
- In good agreement with previous studies we find that the proportion of Seyfert galaxies in our sample increases with warmer FIR colors (S_{60}/S_{25}) and that Seyfert galaxies emit more flux at $25\mu\text{m}$ than starburst galaxies with the same IR luminosity.
- Comparison of the optical spectral types of the galaxies with the radio-FIR observations reveals that the galaxies classified optically as starbursts exhibit a tight radio-FIR correlation with little scatter and a median $q = 2.83$. The galaxies classified optically as Seyferts exhibit a slight (but statistically significant) radio excess on the radio-FIR correlation with a median $q = 2.55$ and a somewhat larger scatter.
- Compact radio cores were detected in 6/11 ($\sim 55\%$) of galaxies classified optically as Seyferts and 3/59 ($\sim 5\%$) of starburst galaxies. The upper limits on the detection of the compact cores in the remaining Seyferts (5/11) are between $10^{3.5}$ to $10^{3.7} L_{\odot}$ indicating that their compact cores, if present, must be at the lower end of the luminosities detected ($10^{3.4}$ – $10^{5.6} L_{\odot}$).
- All the Seyfert galaxies in which compact cores were detected lie significantly above the mean radio-FIR correlation with a median $q = 2.26$. This radio excess is attributed to pc- to kpc-scale radio structures, because the compact radio emission is only a small part of the observed excess (see Paper I). The Seyfert galaxies without compact cores do not exhibit the same radio excess as the Seyfert

galaxies with compact cores and have a similar median q ($= 2.79$) to that of the starburst galaxies. This suggests the presence of two different kinds of Seyferts, “radio-excess” Seyferts (these galaxies are not formally radio loud), which exhibit radio cores and a large-scale radio structure, and “radio-quiet” Seyferts, with low luminosity radio cores and a radio continuum dominated by star formation in the host galaxy. We emphasize that both the *optical strength* of the AGN signature seen in the line diagnostic diagrams and the FIR color of the Seyfert galaxies is insensitive to the difference – the radio quiet Seyfert galaxies often have very dominant AGN-signatures in their optical spectra. We are currently investigating what factors might lead to these differences in the properties of the host galaxies.

- It is not clear whether the compact cores detected in the three galaxies classified optically as starbursts are obscured AGN or complexes of RSNe. They do not exhibit a significant radio excess and the luminosities of the compact cores detected ($10^{3.75}$ to $10^{4.25} L_{\odot}$) are consistent with either origin. This degeneracy may be resolved by VLBI or X-ray observations which could reveal the presence of a collimated pc-scale jet or a hard X-ray continuum if the cores are indeed AGN.
- Galaxies classified as ambiguous and borderline in the K01 scheme have little discernible radio excess (median $q = 2.78, 2.83$ respectively), suggesting that they have more in common with starbursts than AGN. Since these galaxies would have been classified as LINERs on the V95 scheme, this would seem to add support to the idea that some LINER objects are metal-rich starbursts.

8. ACKNOWLEDGMENTS

This paper is dedicated to Charlene Anne Heisler (deceased), who was the driving force behind this project for many years. We thank I. Wormleaton for her help with the reduction of the optical spectroscopic data. We thank S. Veilleux for his careful reading of this paper and his suggestions which have greatly improved its clarity. This research has made use of the NASA/IPAC Extragalactic Database (NED) which is operated by the Jet Propulsion Laboratory, California Institute of Technology, under contract with the National Aeronautics and Space Administration. It has also made use of NASA’s Astrophysics Data System Bibliographic Services and of the on-line NRAO VLA Sky Survey database (Condon et al. 1998). EAC is supported by the Anglo-Australian Fellowship and LK is supported by a Harvard-Smithsonian CfA Fellowship. MAD acknowledges the support of the Australian National University and the Australian Research Council through his ARC Australian Federation Fellowship, and under the ARC Discovery project DP0208445. VC would like to acknowledge the partial support of JPL contract 960803. AZ acknowledges partial support from the Chandra grants G01-2116X and G02-3150X.

REFERENCES

Aguero, E. L., Calderon, J. H., Paolantonio, S., & Suarez Boedo, E. 1994, PASP, 106, 978

Baan, W., Salzer, J. J., & Le Winter, R. D. 1998, ApJ, 509, 633

Baldwin, J. A., Phillips, M. M., & Terlevich, R. 1981, PASP, 93, 5

Barth, A. J., & Shields, J. C. 2000, PASP, 112, 753

Beichman, C., et al., 1988, IRAS Catalogs and Atlases, vol. 1, Explanatory Supplement, NASA RP-1190 (Washington, DC: GPO)

Blandford, R. D., & Rees, M. 1992, in Testing the AGN Paradigm, ed. S. S. Holt, S. G. Neff, & C. M. Urry (New York: AIP), 3

Bransford, M. A., Appleton, P. N., Heisler, C. A., Norris, R. P., & Marston, A. P. 1998, ApJ, 497, 133

Bryant, P. M., & Scoville, N. Z. 1999, AJ, 117, 2632

Bushouse, H. A. 1986, PhD thesis, Univ. Illinois

Buta, R. 1995 ApJS, 96, 39

Charmandaris, V., Stacey, G. J., & Gull, G. 2002a, ApJ, 571, 282

Charmandaris, V., et al. 2002b, A&A, 391, 429

Clavel, J., et al. 2000, A&A, 357, 839

Combes, F. 2001, "Fueling the AGN" In Advanced Lectures on the Starburst-AGN Connection, INAOE, ed. I. Arétxaga, D. Kunth, R. Mujica, P 223.

Condon, J. J., Helou, G., Sanders, D. B., & Soifer, B. T. 1996 ApJS, 103, 81

Corbett, E. A., et al. 2002, ApJ, 564, 650 (Paper I)

Dale, D. A., Helou, G., Contursi, A., Silbermann, N. A. & Kolhatkar, S., 2001, ApJ, 549, 215

de Grijp, M. H. K., Miley, G. K., Lub, J., & de Jong T. 1985 Nature, 314, 240

de Grijp, M. H. K., Miley, G. K., & Lub, J. 1987, A&AS, 70, 95

Dopita, M. A., Kewley, L. J., & Sutherland R. 2000, ApJ, 542, 224

Durret, F., & Bergeron, J. 1986, A&A, 1986, 156, 51

Efstathiou, A., & Rowan-Robinson, M. 1995, MNRAS, 273, 649

Fairall, A.P. 1979 MNRAS, 188, 349

Fairall, A.P. 1986 MNRAS, 218, 453

Gardner, F. F., Whiteoak, J. B., Norris, R. P., & Diamond, P. J. 1992, MNRAS, 258, 296

Genzel, R., et al. 1998, ApJ, 498, 579

Hagiwara, Y., Kohno, K., Kawabe, R., & Nakai N. 1997, PASJ, 49, 171

Heckman, T. 1980, A&A, 87, 152

Heisler, C. A., Lumsden, S. L., & Bailey, J. A. 1997, Nature, 385, 700

Heisler, C. A., Norris, R. P., Juancey, D. L., Reynolds, J. E., & King, E. A. 1998, MNRAS, 300, 1111

Hill, T. L., Heisler C. A, Sutherland, R., & Hunstead R. W. 1999, AJ, 117, 111

Helou, G., Soifer, B. T. & Rowan-Robinson, M. 1985, ApJ, 298, 7

Ho, L. C., Filippenko, A. V. & Sargent, W. L. W. 1993, ApJ, 417, 63

Ho, L. C., Filippenko, A. V., Sargent, W. L. W., & Peng, C. Y. 1997a, ApJS, 112, 391

Ho, L. C., Filippenko, A. V., & Sargent, W. L. W. 1997b, ApJ, 487, 591

Ho, L. C. 2002, ApJ, 564, 120

Hwang, C.-Y., Lo, K. Y., Gao, Y., Gruendl, R. A., & Lu, N. Y. 1999, ApJ, 511, L17

Keel, W. C., de Grijp, M. H. K., Miley, G. K., & Zheng, W. 1994, A&A, 283, 791

Keel, W. C. 1996, AJ, 111, 696

Kennicutt, R. C. 1998, ApJ, 498, 541

Kewley, L., Heisler, C. A., Dopita, M. A., Sutherland, R., Norris, R. P., Reynolds, J., & Lumsden, S. 2000, ApJ, 530, 704

Kewley, L. J., Dopita, M. A., Sutherland, R. S., & Heisler, C. A. 2001a, ApJ, 556, 121 (K01)

Kewley, L. J., Heisler, C. A., Dopita, M. A., & Lumsden, S. 2001b, ApJS, 132, 37

Kewley, L. J., et al. 2002 (K02), in prep

Kinney, A. L., Schmitt, H. R., Clarke, C. J., Pringle, J. E., Ulvestad, J. S., & Antonucci, R. R. J. 2000, ApJ, 537, 152

Knappen, J. H., Shlosman, I., & Peletier, R. F. 2000, ApJ, 529, 93

Kormendy, J., & Gebhardt, K. 2001, in AIP conference proceedings, Vol. 586. Edited by J. C. Wheeler & H. Martel, p.363 [astro-ph/0105230]

Laurent, O., Mirabel, I. F., Charmandaris, V., Gallais, P., Madden, S. C., Sauvage, M., Vigroux, L., & Cesarsky, C., 2000, A&A, 359, 887

Lonsdale, C. J., Smith, H. E., & Lonsdale, C. J. 1993, ApJ, 405, 9

Lutz, D., Spoon, H. W. W., Rigopoulou, D., Moorwood, A. F.. M., & Genzel, R. 1998, ApJ, 505, 103

Lutz, D., Veilleux, S., & Genzel, R. 1999, ApJ, 517, L13

Maoz, D., Koratkar, A., Shields, J. C., Ho, L. C., Filippenko, A. V., & Sternberg, A. 1998, AJ, 116, 55

Martin, J. M., Bottinelli, L., Dennefeld, M., Gougenheim, L., & Le Squeren, A. M. 1989, A&A, 208, 39

Martini, P., & Pogge, R. W., 1999, AJ, 118, 2646

Miller, J. S., & Mathews, W. G. 1972, ApJ, 172, 593

Moshir, M., et al. 1990, IRAS Faint Source Catalogue, ver. 2.0.

Murphy, T. W., Soifer, B. T., Matthews, K., Kiger, J. R. & Armus, L. 1999, ApJ, 525, 85

Norris, R. P., Allen, D. A., Sramek, R. A., Kesteven, M. J. & Troup, E. R. 1990, ApJ, 359, 291.

Phillips, M. M., Charles, P. A., & Baldwin, J. A. 1983, ApJ, 266, 485

Pier, E. A., & Krolik, J. H. 1993, ApJ418, 673

Roy, A. L., Norris, R. P., Kesteven, M. J., Troup, R. R. & Reynolds, J. E. 1998, MNRAS, 301, 1019.

Sandage, A., & Brucato, R. 1979, AJ, 84, 472

Sanders, D. B., & Mirabel, I. F. 1996, ARA&A, 34, 749

Sanders, D. B., & Mirabel, I. F. 1985, ApJ, 298, 31

Sanders, D. B., Soifer, B. T., Elias, J. H., Madore, B. F., Matthews, K., Neugebauer, G., & Scoville, N. Z. 1988, ApJ, 325, 74

Smith, H. E., Lonsdale, C. J., & Lonsdale, C. J. 1998a, ApJ, 492, 137 (SLL98)

Smith, H. E., Lonsdale, C. J., Lonsdale, C. J., & Diamond, P. J. 1998, ApJ, 493, 17

Strauss, M. A., Huchra, J. P., Davis, M., Yahil, A., Fisher, K. B., & Tonry, J. 1992, ApJS, 83, 29

Thean, A., Pedlar, A., Kukula, M. J., Baum, S. A., & O'Dea, C. P. 2000, MNRAS, 314, 573

Thuan, T.X. 1984, ApJ, 281, 126

Tran, Q. H., et al. 2001, ApJ, 552, 527

Vaceli, M. S., Viegas, S. M., Gruenwald, R., & de Souza, R. E. 1997, AJ, 114, 1345

Veilleux, S., & Osterbrock D. E. ApJS, 1987, 63 259 (VO87)

Veilleux, S., Kim, D.-C., Sanders, D. B., Mazzarella, J. M., & Soifer, B. T. 1995, ApJS, 98, 171 (V95)

Veilleux, S., Kim, D.-C., & Sanders, D. B. 1999, ApJ, 522, 113 (V99)

Wu, H., Zou, Z. L., Xia, X. Y., & Deng, Z. G. 1998, A&AS, 132, 181

Yun, M. S., & Hibbard, J. E. 2001, ApJ, 550, 104

TABLE 1

THE OBSERVED LINE RATIOS AND OPTICAL CLASSIFICATIONS FOR THE COLA SAMPLE.

IRAS Name	ap.	Ref	$\frac{H\alpha}{H\beta}$	E(B-V)	$\frac{[OIII]}{H\beta}$	$\frac{[NII]}{H\alpha}$	$\frac{[SII]}{H\alpha}$	$\frac{[OI]}{H\alpha}$	V95	$\frac{[NII]}{H\alpha}$	V95	$\frac{[SII]}{H\alpha}$	V95	$\frac{[OI]}{H\alpha}$	Final Class	K01	$\frac{[NII]}{H\alpha}$	K01	$\frac{[SII]}{H\alpha}$	K01	$\frac{[OI]}{H\alpha}$	K01	Final Class
(1)	(2)	(3)	(4)	(5)	(6)	(7)	(8)	(9)	(10)	(11)	(12)	(13)	(14)	(15)	(16)	(17)							
00085-1223	1	1.12	1.45	0.01	0.10	-0.49	-1.32	L	HII	HII	AMB	AGN	HII	HII	HII	AMB							
00344-3349	1	2	...	0.50	-0.79	-0.87	-1.74	HII	HII	HII	HII	HII	HII	HII	HII	HII							
00344-3349	2	2	...	0.48	-0.75	-0.77	-1.67	HII	HII	HII	HII	HII	HII	HII						
00402-2350	1	0.61	0.26	-0.23	-0.10	L	L	HII	HII						
01053-1746	1	0.59	0.31	0.08	-0.53	...	HII	HII	HII	HII	HII						
01159-4443	2	1	0.89	0.91	0.26	-0.34	...	-0.94	B(HII)	...	L	B	HII	...	AGN	AMB							
01159-4443	1	1	1.13	1.56	-0.17	-0.30	...	-1.43	HII	...	HII	HII	HII	HII	HII	HII	HII						
01165-1719	1	0.87	0.96	-0.20	-0.47	-0.58	-1.53	HII	HII	HII	HII	HII	HII	HII	HII	HII	HII						
01326-3623	1	No lines	No lines						
01341-3734	1	2	0.67	0.41	-0.39	-0.29	-0.65	-1.63	HII	HII	HII	HII	HII	HII	HII	HII	HII						
01341-3734	2	2	0.57	0.17	-0.20	-0.30	-0.66	-1.63	HII	HII	HII	HII	HII	HII	HII	HII	HII						
01384-7515	1	0.88	0.97	-0.33	-0.28	-0.55	-1.42	HII	HII	HII	HII	HII	HII	HII	HII	HII	HII						
02015-2333	2	0.79	0.69	-0.63	-0.28	-0.60	-1.62	HII	HII	HII	HII	HII	HII	HII	HII	HII	HII						
02069-1022	1	0.68	0.43	-0.17	-0.03	-0.42	L	B(HII)	...	B	B(HII)	HII	HII	HII							
02072-1025	1	1.10	1.40	0.13	-0.23	-0.49	-1.24	B(A)	B(HII)	B(A)	B	HII	HII	B(HII)	HII	HII							
02140-1134	1	0.83	0.87	-0.44	-0.31	-0.65	HII	HII	...	HII	HII	HII	HII	...	HII	HII							
02281-0309	1	0.14	H abs	H abs	H abs							
02433-1534	1	1.04	1.28	-0.18	-0.33	-0.54	-1.05	HII	HII	L	AMB	HII	HII	B(A)	HII								
02436-5556	1	-0.13	-0.96	N	No lines	No lines							
02476-3858	1	N	No lines							
03022-1232	1	1.26	1.77	0.48	-0.13	-0.45	AGN	AGN	Sy	AGN	AGN	AGN	AGN	AGN	AGN	AGN							
04118-3207	1	0.66	0.38	0.44	-0.12	-0.54	-1.40	L	B(HII)	B	AGN	B(A)	B(A)	B	B								
04210-4042	1	0.72	0.60	-0.66	-0.30	-0.70	-1.59	HII	HII	HII	HII	HII	HII	HII	HII	HII							
04315-0840	2	1.11	1.43	-0.09	-0.22	-0.64	-1.76	B(A)	HII	HII	HII	HII	...	HII	HII	HII							
04335-2514	1	0.04	-0.37	H abs	H abs	H abs							
04370-2416	1	0.59	0.32	-0.61	-0.47	-0.57	-1.57	HII	HII	HII	HII	HII	HII	HII	HII	HII							
04461-0624	1	0.45	0.00	1.08	0.52	0.27	-0.28	AGN	AGN	AGN	Sy2 ¹	AGN	AGN	AGN	AGN ¹	AGN ¹							
04501-3304	1	0.99	1.15	-0.57	-0.14	-0.79	L	HII	AMB	HII	HII	HII	HII							
04558-0751	1	-0.05	-0.60	No Lines	No lines	No lines							
04569-0756	1	-0.15	-0.46	H abs	H abs	H abs							
04591-0419	1	0.42	0.00	0.45	-1.03	-0.87	-1.96	HII	HII	HII	HII	HII	HII	HII	HII	HII							
04595-1813	1	0.69	0.54	-0.10	-0.49	-0.51	HII	HII	...	HII	HII	HII	HII	...	HII	HII							
05041-4938	1	0.84	0.89	-0.38	-0.51	-0.73	HII	HII	...	HII	HII	HII	HII	...	HII	HII							
05053-0805	2	0.95	1.06	-0.73	-0.31	-0.61	-1.64	HII	HII	HII	HII	HII	HII	HII	HII	HII							
05140-6213	1	0.80	0.79	-0.14	-0.37	-0.67	HII	HII	...	HII	HII	HII	HII	...	HII	HII							
05449-0651	1	-0.39	No lines	No lines	No lines							
05562-6933	1	0.69	0.53	-0.54	-0.29	-0.61	-1.58	HII	HII	HII	HII	HII	HII	HII	HII	HII							
06295-1735	1	0.63	0.40	-0.35	-0.38	-0.58	-1.49	HII	HII	HII	HII	HII	HII	HII	HII	HII							
06592-6313	2	1.07	1.34	-0.60	-0.10	-0.61	-1.39	L	HII	HII	AMB	HII	HII	HII	HII	HII							
08175-1433	1	0.67	0.49	...	-0.40	-0.78	-1.96	No lines	No lines	No lines							
08225-6936	1	0.80	0.80	-0.45	-0.30	-0.62	HII	HII	HII	HII	HII	HII	HII	HII	HII	HII							
08364-1430	1	0.70	0.56	-0.43	-0.33	-0.44	-1.53	HII	B(HII)	HII	HII	HII	HII	HII	HII	HII							
08438-1510	2	1.11	1.42	0.15	-0.17	-0.38	-1.11	L	L	L	B(HII)	B(HII)	B(HII)	B(HII)	B								
09006-6404	1	0.72	0.61	0.28	-0.41	-0.53	-1.43	HII	B(HII)	HII	HII	HII	HII	HII	HII	HII							
09248-1918	2	0.92	0.98	-0.42	-0.21	-0.51	-1.47	B(A)	HII	HII	HII	HII	HII	HII	HII	HII							
09375-6951	1	1	0.98	1.14	-0.22	-0.26	-0.42	B(HII)	B(HII)	B	HII	HII	HII	HII	HII	HII							
09375-6951	2	1	0.75	0.67	-0.50	-0.36	-0.51	-1.19	HII	HII	B(HII)	HII	HII	HII	HII	HII							
10015-0614	1	1	0.81	0.82	-0.59	-0.37	-0.70	-1.59	HII	HII	HII	HII	HII	HII	HII	HII							
10015-0614	2	1	0.59	0.30	-0.36	-0.49	-0.64	-1.78	HII	HII	HII	HII	HII	HII	HII	HII							
10221-2317	1	0.80	0.72	0.13	-0.09	-0.46	-1.33	L	B(HII)	HII	B	B(A)	HII	HII	HII	HII							
10409-4457	1	0.68	0.44	-0.03	-0.11	...	L	L	HII	HII	HII	HII							
10484-0153	1	0.52	0.16	-0.88	-0.36	-0.48	-1.46	HII	HII	HII	HII	HII	HII	HII	HII	HII							
10567-4310	1	0.95	1.14	<-0.77	-0.31	-0.73	-1.67	HII	HII	HII	No OIII	HII	HII	HII	No OIII	No OIII							
11005-1601	1	0.77	0.72	-0.72	-0.35	-0.56	-1.71	HII	HII	HII	HII	HII	HII	HII	HII	HII							
11254-4120	1	0.87	0.87	-0.44	-0.04	-0.57	-1.33	L	HII	HII	AMB	HII	HII	HII	HII	HII							
11328-4844	1	-0.11	-0.38	-1.06	H abs	H abs	H abs							
11409-1631	2	0.58	0.20	-0.15	-0.59	-0.54	-1.70	HII	HII	HII	HII	HII	HII	HII	HII	HII							
12042-3140	1	1	0.43	0.00	-0.05	-0.25	...	-0.33	B(HII)	...	L	B	HII	...	L	AMB							
12042-3140	2	1	0.90	1.02	-0.27	-0.44	HII	HII	HII	HII							

TABLE 1—Continued

IRAS Name	ap.	Ref	$\frac{H\alpha}{H\beta}$	E(B-V)	$\frac{[OIII]}{H\beta}$	$\frac{[NII]}{H\alpha}$	$\frac{[SII]}{H\alpha}$	$\frac{[OI]}{H\alpha}$	V95	$\frac{[NII]}{H\alpha}$	V95	$\frac{[SII]}{H\alpha}$	V95 Final	Class	K01	$\frac{[NII]}{H\alpha}$	K01	$\frac{[SII]}{H\alpha}$	K01	$\frac{[OI]}{H\alpha}$	K01 Final	Class
(1)	(2)	(3)	(4)	(5)	(6)	(7)	(8)	(9)	(10)	(11)	(12)	(13)	(14)	(15)	(16)	(17)						
12112-4659	1	0.92	1.08	-0.52	-0.30	-0.66	-1.90	HII	HII	HII	HII	HII	HII	HII	HII	HII	HII	HII	HII	HII		
12115-4657	1	0.72	0.60	0.04	-0.31	-0.60	-1.78	HII	HII	HII	HII	HII	HII	HII	HII	HII	HII	HII	HII	HII		
12120-1118	1	0.71	0.60	-0.50	-0.39	-0.53	-1.52	HII	HII	HII	HII	HII	HII	HII	HII	HII	HII	HII	HII	HII		
12171-1156	1	0.73	0.64	-0.72	-0.35	-0.60	...	HII	HII	...	HII	HII	HII	HII	...	HII	...	HII	...	HII	HII	
12286-2600	2	0.89	0.93	-0.64	-0.24	-0.66	-1.64	B(HII)	HII	HII	HII	HII	HII	HII	HII	HII	HII	HII	HII	HII	HII	
12329-3938	1	0.47	0	0.93	-0.29	-0.43	-0.93	AGN	AGN	AGN	Sy2	AGN	AGN	AGN	AGN	AGN	AGN	AGN	AGN	AGN	AGN	
12351-4015	1	1	0.65	0.37	-0.22	-0.51	-0.57	-0.26	HII	HII	L	AMB	HII	HII	HII	L	AMB	HII	HII	HII	HII	
12351-4015	3	1	0.70	0.47	-0.60	-0.28	-0.50	-0.95	HII	HII	L	AMB	HII	HII	B(A)	HII	HII	HII	HII	HII	HII	
12351-4015	2	1	0.73	0.63	-0.61	-0.50	-0.57	-1.36	HII	HII	HII	HII	HII	HII	HII	HII	HII	HII	HII	HII	HII	
12596-1529	1	2	0.97	1.10	-0.35	-0.28	-0.62	-1.49	HII	HII	HII	HII	HII	HII	HII	HII	HII	HII	HII	HII	HII	
12596-1529	2	2	0.79	0.70	-0.15	-0.49	-0.65	-1.85	HII	HII	HII	HII	HII	HII	HII	HII	HII	HII	HII	HII	HII	
12596-1529	3	2	0.72	0.53	0.10	-0.68	-0.55	-1.48	HII	HII	HII	HII	HII	HII	HII	HII	HII	HII	HII	HII	HII	
13001-2339	1	0.83	0.78	-0.11	-0.13	...	-0.84	L	...	L	L	HII	...	AGN	AGN	AMB	AGN	AGN	AGN	AGN	AGN	
13035-4008	1	0.59	0.22	0.75	0.15	-0.01	...	AGN	Sy1 ²	AGN	AGN	AGN	AGN	AGN	AGN	AGN	AGN	AGN	AGN	
13097-1531	1	0.61	0.28	-0.46	-0.20	-0.45	-1.25	B(A)	B(HII)	HII	B	HII	HII	HII	HII	HII	HII	HII	HII	HII	HII	
13135-2801	1	0.79	0.77	-0.58	-0.30	-0.67	...	HII	HII	...	HII	HII	HII	HII	HII	HII	HII	HII	HII	HII	HII	
13192-5208	1	0.82	0.84	-0.63	-0.32	-0.66	...	HII	HII	...	HII	HII	HII	HII	HII	HII	HII	HII	HII	HII	HII	
13197-1627	1	1.30	0.69	0.51	0.23	AGN	AGN	AGN	Sy1 ^{8,3}	AGN	AGN	AGN	AGN	AGN	AGN	AGN	AGN	AGN	AGN	
13229-2934	2	0.71	0.51	0.69	-0.04	-0.45	-1.19	AGN	AGN	AGN	Sy2	AGN	AGN	AGN	AGN	AGN	AGN	AGN	AGN	AGN	AGN	
14544-4255	1	0.64	0.35	0.81	-0.14	-0.23	-0.93	AGN	AGN	AGN	Sy2	AGN	AGN	AGN	AGN	AGN	AGN	AGN	AGN	AGN	AGN	
14566-1629	1	1.01	1.20	0.57	0.08	-0.23	...	AGN	AGN	...	Sy2	AGN	AGN	AGN	AGN	AGN	AGN	AGN	AGN	AGN	AGN	
15555-6610	1	0.76	0.62	1.10	-0.01	-0.34	-0.85	AGN	AGN	AGN	Sy2	AGN	AGN	AGN	AGN	AGN	AGN	AGN	AGN	AGN	AGN	
16153-7001	1	No lines	No lines	
16229-6640	1	1	1.25	1.76	-0.09	-0.15	...	-1.32	L	...	HII	AMB	HII	HII	HII	HII	HII	HII	HII	HII	HII	
16229-6640	2	1	0.88	0.97	-0.52	-0.28	...	HII	HII	...	HII	HII	HII	HII	HII	HII	HII	HII	HII	HII	HII	
17138-1017	2	1.41	2.12	-0.34	-0.29	-0.54	-1.37	HII	HII	HII	HII	HII	HII	HII	HII	HII	HII	HII	HII	HII	HII	
17182-7353	1	N	N	...	
17260-7622	1	0.82	0.83	-0.18	-0.45	-0.50	...	HII	HII	...	HII	HII	HII	HII	HII	HII	HII	HII	HII	HII	HII	
18093-5744	1	0.68	0.52	-0.28	-0.35	-0.53	-1.52	HII	HII	HII	HII	HII	HII	HII	HII	HII	HII	HII	HII	HII	HII	
18293-3413	1	1.25	1.82	...	-0.31	...	-1.32	N	No lines	
18341-5732	1	1.19	1.61	-0.24	-0.12	-0.57	-1.44	L	HII	HII	AMB	HII	HII	HII	HII	HII	HII	HII	HII	HII	HII	
18421-5049	1	0.13	0	0.08	-0.12	-0.46	...	B(HII)	B	B(HII)	B(HII)	HII	HII	HII	HII	HII	HII	HII	HII	HII	HII	
18429-6312	2	0.86	0.85	1.12	-0.09	-0.38	-1.00	AGN	AGN	AGN	Sy2	AGN	AGN	AGN	AGN	AGN	AGN	AGN	AGN	AGN	AGN	
19543-3804	1	1.09	1.38	0.99	0.14	-0.26	-0.74	AGN	AGN	AGN	Sy	AGN	AGN	AGN	AGN	AGN	AGN	AGN	AGN	AGN	AGN	
20305-0211	2	1	0.69	0.53	-0.28	-0.53	-0.64	-1.67	HII	HII	HII	HII	HII	HII	HII	HII	HII	HII	HII	HII	HII	
20305-0211	1	1	0.77	0.72	-0.08	-0.50	-0.76	-1.30	HII	HII	HII	HII	HII	HII	HII	HII	HII	HII	HII	HII	HII	
20309-1132	1	0.75	0.67	-0.48	-0.45	-0.51	...	HII	HII	...	HII	HII	HII	HII	HII	HII	HII	HII	HII	HII	HII	
20486-4857	1	0.14	H abs	H abs	...	
21008-4347	1	0.13	...	-0.38	-0.41	HII	HII	HII	...	
21314-4102	1	0.81	0.73	-0.29	-0.12	...	-0.84	L	...	L	L	HII	...	AGN	AGN	AMB	AGN	AGN	AGN	AGN	AGN	
21330-3846	2	2	1.10	1.41	-0.24	-0.37	-0.65	-1.21	HII	HII	B(HII)	HII	HII	HII	HII	HII	HII	HII	HII	HII	HII	
21330-3846	1	2	0.83	0.78	-0.18	-0.17	-0.30	...	L	L	...	L	HII	HII	HII	HII	HII	HII	HII	HII	HII	HII
21453-3511	1	0.79	0.69	0.80	-0.17	-0.45	-0.86	AGN	AGN	AGN	Sy	AGN	AGN	AGN	AGN	AGN	AGN	AGN	AGN	AGN	AGN	
22115-3013	1	0.77	0.73	-0.48	-0.36	-0.55	...	HII	HII	...	HII	HII	HII	HII	HII	HII	HII	HII	HII	HII	HII	
22118-2742	1	0.79	0.77	-0.19	-0.44	HII	HII	HII	HII	HII	HII	HII	HII	HII	HII	HII	HII	
22179-2455	1	0.81	0.82	...	-0.26	-0.51	No lines	No lines	
23394-0353	1	0.92	1.08	-0.35	-0.36	-0.61	-1.36	HII	HII	HII	HII	HII	HII	HII	HII	HII	HII	HII	HII	HII	HII	

Note. — Column 2 identifies the aperture for those galaxies which exhibited multiple “hotspots”. Column 3 indicates whether the galaxy spectrum was obtained as part of this work (1) or K01 (2). The logarithm of the line ratios is given in columns 4 and 6-9. The values quoted in column 4 are before the data were corrected for extinction along the line of sight whereas the line ratios quoted in columns 6-9 are extinction corrected. The errors in the line ratios vary from object to object but typical errors are ± 0.017 dex for $\text{Log}([\text{OIII}]/\text{H}\beta)$, ± 0.005 dex for $\text{Log}([\text{NII}]/\text{H}\alpha)$, 0.005 dex for $\text{Log}([\text{SII}]/\text{H}\alpha)$ and ± 0.04 dex for $\text{Log}([\text{OI}]/\text{H}\alpha)$ to be ± 0.04 dex. The optical classifications of the galaxies from the V95 scheme are given in columns 10-12 and those using the K01 scheme are shown in columns 14-17. Classifications are as follows: Sy=Seyfert, HII=starburst, AMB=ambiguous classification, B=galaxy lies within 0.5 dex of the AGN/HII partition, AGN=AGN (probably Seyfert), L=LINER. See text for more details. Notes are as follows: ¹ All “narrow” emission lines unusually broad (FWHM $\sim 1000 \text{ km s}^{-1}$); ² Broad H α and H β detected; ³ Additional broad H α component detected (FWHM $\sim 2000 \text{ km s}^{-1}$), but no additional broad H β component.

TABLE 2

THE CLASSIFICATION STATISTICS FOR THE COLA GALAXIES USING THE V95 AND K01 SCHEMES.

Class	V95 Nuclear	V95 All Ap.	K01 Nuclear	K01 All Ap.
HII	44	54	59	70
AGN	12	12	12	12
LINERs	6	6	0	0
B	8	9	2	2
AMB	7	9	4	6
Not classified	15	15	15	15
Total	93	106	93	106

Note. — “Nuclear” classification refers to the classification of the nuclear spectrum of each galaxy. “All apertures” includes additional spectra from “hotspots” detected in some of the galaxies.

TABLE 3

THE MINIMUM AND MAXIMUM PERCENTAGE CONTRIBUTION TO THE OBSERVED EMISSION LINE RATIOS DUE TO IONIZATION OF THE GAS BY AN AGN CONTINUUM. THIS IS CALCULATED USING THE THEORETICAL IONIZATION MODELS OF K01 WITH IONIZATION BY STARBURST ACTIVITY ACCOUNTING FOR THE REMAINDER OF THE LINE RATIOS (SEE DISCUSSION IN TEXT FOR FURTHER DETAILS).

Names	ap.	[NII]/H α (%)	[SII]/H α (%)	[OI]/H α (%)	Mean (%)	Min (%)	Max (%)
00085-1223		15-20	0-15	0-15	11	0	20
00344-3349	1	10-10	0-10	0-5	4	0	10
00344-3349	2						
00402-2350		0-10	0-10		5	0	10
01053-1746		0-5	0-15		5	0	15
01159-4443	2	0-10	0-10	0-10	5	0	10
01159-4443	1	0-15	0-25	20-30	15	0	30
01165-1719		0-5	0-10	0-10	6	0	10
01326-3623							
01341-3734	1	0-10	0-10	0-5	4	0	10
01341-3734	2	0-10	0-10	0-10	5	0	10
01384-7515		0-5	0-10	0-10	6	0	10
02015-2333		0-5	0-5	0-5	3	0	5
02069-1022		0-10	0-10		5	0	10
02072-1025		0-15	0-20	0-20	9	0	20
02140-1134		0-5	0-10		4	0	10
02281-0309							
02433-1534		0-10	0-5	0-10	6	0	10
02436-5556							
02476-3858							
03022-1232*		10-30	10-50		25	10	50
04118-3207		10-30	0-40	0-15	16	0	40
04210-4042		0-5	0-5	0-5	3	0	5
04315-0840		0-15	0-10	0-5	6	0	15
04335-2514							
04370-2416		0-5	0-5	0-5	3	0	5
04461-0624*		100	100	100	100	100	100
04501-3304		0-5	0-5		3	0	5
04558-0751							
04569-0756							
04591-0419		0-0	0-10	0-5	3	0	10
04595-1813		0-5	0-10		4	0	10
05041-4938		0-5	0-5		3	0	5
05053-0805		0-5	0-0	0-5	2	0	5
05140-6213		0-10	0-10		5	0	10
05449-0651							
05562-6933		0-5	0-5	0-5	3	0	5
06295-1735		0-10	0-10	0-10	5	0	10
06592-6313		0-5	0-5	0-5	3	0	5
08175-1433							
08225-6936		0-5		0-5	3	0	5
08364-1430		0-5	0-5	0-10	3	0	10
08438-1510		0-10	0-40	0-15	11	0	40
09006-6404		0-10	0-40	0-15	11	0	40
09248-1918		0-5	0-10	0-10	4	0	10
09375-6951	1	0-10	0-10		5	0	10
09375-6951	2	0-5	0-5	0-5	3	0	5
10015-0614	1	0-5	0-5	0-5	3	0	5
10015-0614	2	0-5	0-10	0-5	3	0	10
10221-2317		0-20	0-20	0-20	10	0	20
10409-4557		0-15	0-15		8	0	15
10484-0153		0-0	0-0	0-0	0	0	0
10567-4310							
11005-1601		0-5	0-5	0-5	3	0	5
11254-4120		0-5	0-5	0-10	3	0	10
11328-4844							
11409-1631		0-5	0-10	0-5	3	0	10
12042-3140	1	0-15		LINER	8	0	15
12042-3140	2	0-10			5	0	10
12112-4659		0-5	0-5	0-5	3	0	5
12115-4657		0-10	0-20	0-5	6	0	20
12120-1118		0-5	0-5	0-5	3	0	5
12171-1156		0-5	0-5		3	0	5
12286-2600		0-5	0-5	0-5	3	0	5
12329-3938*		80-100	70-100	100	92	70	100
12351-4015	1	0-5	0-5	0-5	3	0	5

TABLE 3—*Continued*

Names	ap.	[NII]/H α (%)	[SII]/H α (%)	[OI]/H α (%)	Mean (%)	Min (%)	Max (%)
12351-4015	3	0-5	0-10	LINER	4	0	10
12351-4015	2	0-5	0-5	0-5	3	0	5
12596-1529	1	0-10	0-5	0-5	3	0	10
12596-1529	2	0-5	0-10	0-5	3	0	10
12596-1529	3	0-0	0-20	0-10	8	0	20
13001-2339		0-10	10-30	LINER	7	0	10
13035-4008*		50-60	100		78	50	100
13097-1531		0-5	0-5	0-10	3	0	5
13135-2801		0-5	0-5		3	0	5
13192-5208		0-5	0-5		3	0	5
13197-1627*		100	100	100	100	100	100
13229-2934*		30-40	25-50	10-20	31	10	50
14544-4255*		40-50	80-100	30-40	57	40	100
14566-1629*		30-50	40-50		43	30	50
15555-6610*		100	100	100	100	100	100
16153-7001							
16229-6640	1	0-5	0-5		3	0	5
16229-6640	2	0-5			3	0	5
17138-1017		10-10	0-10	0-5	4	0	10
17182-7353							
17260-7622		0-10	0-10		5	0	10
18093-5744		0-10	0-10	0-10	5	0	10
18293-3413							
18341-5732		0-10	0-10	0-10	5	0	10
18421-5049		0-20	0-20		10	0	20
18429-6312*		100	100	100	100	100	100
19543-3804*		80-100	90-100	100	95	80	100
20305-0211	1	0-5	0-10	0-5	7	0	10
20305-0211	3	0-5	0-10	0-10	8	0	10
20309-1132		0-5	0-5		3	0	5
20486-4857							
21008-4347		0-5	0-5		3	0	5
21314-4102		0-5	0-10	L			
21330-3846	2	0-10	0-10	0-10	5	0	10
21330-3846	1	0-10	0-10		5	0	10
21453-3511*		40-45	35-50	40-50	43	35	50
22115-3013		0-5	0-5		3	0	10
22118-2742		0-10	0-10		5	0	10
22179-2455							
23394-0353		0-5	0-5	0-10	7	0	10

Note. — Galaxies which are classed as Sy1 or Sy2 in both the V95 and K01 classification schemes are marked with an asterix.

TABLE 4
THE MULTI-WAVELENGTH PROPERTIES OF THE GALAXIES.

Name (1)	Vel. (2)	D (3)	S ₁₂ (4)	S ₂₅ (5)	S ₆₀ (6)	S ₁₀₀ (7)	$\frac{S_{60}}{S_{25}}$ (8)	Log($\frac{L_{LR}}{L_{\odot}}$) (9)	P _{FIR} (10)	P _{4.8} (11)	q (12)	S _{LB} A (13)	V95 Class (14)	K01 Class (15)
00085-1223	5821	77.99	0.40	2.37	16.60	17.20	7.00	11.42	14.67	2.15	2.83	<2.3	AMB	AMB
00344-3349	6156	82.50	0.42	2.49	6.48	5.01	2.60	11.18	5.94	1.24	2.68	<1.5	HII/HII	HII/HII
00402-2350	6647	89.12	0.33	1.08	10.00	18.30	9.26	11.37	14.07	2.17	2.81	<2.6	L	HII
01053-1746	6016	80.62	0.68	3.57	22.60	30.40	6.33	11.62	23.17	5.80	2.60	<1.7	HII	HII
01159-4443	6701	89.85	0.30	1.86	7.84	11.70	4.22	11.31	10.36	2.08	2.70	<1.4	HII/B	HII/AMB
01165-1719	5977	80.09	0.19	0.63	4.06	6.99	6.44	10.92	4.50	0.87	2.72	<1.7	HII	HII
01326-3623	4827	64.62	0.26	0.68	7.29	15.80	10.77	10.98	5.81	1.53	2.58	<1.9	N	N
01341-3734	5180	69.37	0.27	0.69	5.39	12.80	7.87	10.95	5.16	0.60	2.94	<1.8	HII/HII	HII/HII
01384-7515	3966	53.05	0.33	0.81	7.28	13.80	8.98	10.81	3.69	0.52	2.85	<1.1	HII	HII
02015-2333	4934	66.06	0.20	0.76	4.02	7.32	5.31	10.77	3.10	0.51	2.78	<2.7	HII	HII
02069-1022	4152	55.55	0.35	0.45	5.31	17.70	11.77	10.82	3.89	0.46	2.93	<1.9	B	HII
02072-1025	3847	51.46	0.45	2.48	10.60	23.60	4.27	11.01	5.42	0.62	2.94	<1.6	B	HII
02140-1134	4009	53.63	0.44	0.75	5.97	11.80	7.98	10.77	3.14	0.55	2.76	<2.2	HII	HII
02281-0309	5738	76.87	0.47	0.53	5.25	15.60	10.00	11.10	6.92	1.44	2.68	<1.9	N	N
02433-1534	4101	54.87	0.32	0.68	7.12	13.80	10.47	10.82	3.89	0.73	2.73	<1.8	AMB	HII
02436-5556	5507	73.76	0.29	0.44	4.66	11.40	10.66	10.95	5.12	0.72	2.85	<1.8	N	N
02476-3858	5008	67.05	0.08	0.33	4.47	6.68	13.59	10.72	3.29	0.34	2.99	<1.8	N	N
03022-1232	4282	57.30	0.27	0.99	7.76	10.60	7.85	10.85	4.04	0.55	2.87	<1.6	Sy2	Sy2
04118-3207	3570	47.74	0.53	2.13	14.20	21.60	6.67	10.98	5.33	0.71	2.88	<2.2	B	B(AGN)
04210-4042	6012	80.56	0.23	0.78	8.01	16.40	10.32	11.20	9.67	1.42	2.83	<1.9	HII	HII
04315-0840	4744	63.50	1.44	7.29	32.30	32.70	4.43	11.59	18.80	3.06	2.79	<2.8	HII	HII
04335-2514	4843	64.83	0.17	0.43	4.99	9.75	11.63	10.80	3.82	0.80	2.68	<2.5	N	N
04370-2416	4422	59.18	0.34	0.57	6.00	11.00	10.51	10.82	3.73	0.66	2.75	<1.5	HII	HII
04461-0624	4578	61.27	0.43	0.68	5.95	14.70	8.79	10.91	4.53	1.06	2.63	<1.8	Sy2	Sy2
04502-3304	5622	75.31	0.20	1.18	8.39	9.40	7.11	11.10	7.08	0.61	3.06	<1.6	AMB	HII
04558-0751	3773	50.47	0.20	0.60	5.94	10.10	9.85	10.64	2.60	0.41	2.80	<1.4	N	N
04569-0756	4242	56.76	0.29	0.71	6.78	13.60	9.55	10.84	4.03	0.55	2.87	<2.7	N	N
04591-0419	4068	54.42	0.11	0.58	3.92	5.84	6.77	10.52	1.90	0.34	2.74	<1.5	HII	HII
04595-1813	3978	53.22	0.19	0.34	4.05	8.78	12.05	10.57	2.19	0.40	2.74	<2.3	HII	HII
05041-4938	4145	55.46	0.25	0.29	3.07	7.88	10.70	10.54	1.95	0.10	3.28	<1.6	HII	HII
05053-0805	4478	59.93	0.33	1.33	8.26	13.30	6.21	10.96	5.00	0.46	3.03	NObs	HII	HII
05140-6213	4966	66.49	0.18	0.33	2.78	10.20	8.53	10.72	3.09	0.20	3.19	<1.7	HII	HII
05449-0651	6467	86.69	0.25	0.25	0.85	6.02	3.40	10.73	2.48	ND	...	<1.7	N	N
05562-6933	4440	59.42	0.27	0.58	4.48	15.10	7.74	10.81	3.78	0.45	2.92	<1.7	HII	HII
06295-1735	6339	84.97	0.11	0.56	6.36	9.12	11.44	11.08	7.41	0.78	2.98	<1.5	HII	HII
06592-6313	6882	92.29	0.16	0.80	5.74	7.56	7.20	11.13	7.66	0.88	2.94	<2.6	AMB	HII
08175-1433	5732	76.79	0.21	0.56	4.63	9.02	8.33	10.94	4.97	1.13	2.64	<1.3	N	N
08225-6936	3924	52.49	0.20	0.67	4.72	6.41	7.00	10.58	2.06	0.29	2.85	<1.7	HII	HII
08364-1430	4184	55.98	0.46	0.46	4.23	7.40	9.18	10.67	2.31	0.46	2.70	<1.3	HII	HII
08438-1510	5423	72.63	0.13	0.57	4.11	5.63	7.17	10.79	3.44	0.57	2.78	<2.1	L	B(HII)
09006-6404	6636	88.97	0.15	0.48	3.87	5.88	8.00	10.95	5.05	1.09	2.67	<1.6	HII	HII
09248-1918	4888	65.44	0.15	0.56	4.16	7.61	7.50	10.74	3.16	0.51	2.80	<2.5	HII	HII
09375-6951	6066	81.29	0.20	0.41	4.34	9.68	10.48	10.97	5.54	1.38	2.61	3.6	B/HII	HII/HII
10015-0614	5034	67.40	0.59	1.04	10.70	19.20	10.29	11.18	8.54	2.06	2.62	<1.6	HII/HII	HII/HII
10221-2317	3662	48.98	0.30	1.20	11.20	14.80	9.33	10.85	4.21	0.65	2.81	<2.7	B	HII
10409-4557	7000	93.88	0.37	0.64	5.28	12.60	8.26	11.22	9.29	1.42	2.82	<1.7	L	HII
10484-0153	4464	59.74	0.28	0.54	4.51	9.83	8.29	10.74	3.08	ND	...	<1.3	HII	HII
10567-4310	5156	69.04	0.35	0.80	5.76	10.40	7.17	10.95	4.84	0.64	2.88	<1.6	N	N
11005-1601	3877	51.86	0.41	0.89	6.75	14.00	7.55	10.79	3.40	0.55	2.79	<2.6	HII	HII
11254-4120	4902	65.63	0.20	0.81	8.06	8.41	9.94	10.93	5.05	0.53	2.98	<1.3	AMB	HII
11328-4844	5624	75.34	0.20	0.43	4.01	7.11	9.33	10.84	3.98	0.90	2.65	<1.6	N	N
11409-1631	3660	48.95	0.21	0.63	4.20	7.01	6.71	10.50	1.72	0.24	2.86	<1.6	HII	HII
12042-3140	6818	91.42	0.25	0.68	7.56	11.40	11.13	11.24	10.38	1.91	2.74	<1.7	B/HII	AMB/HII
12112-4659	5493	73.58	0.19	0.66	4.71	6.81	7.15	10.87	4.12	0.46	2.95	<1.5	HII	HII
12115-4657	5543	74.25	0.32	0.66	5.23	9.00	7.90	10.96	4.98	1.19	2.62	<1.7	HII	HII
12120-1118	5406	72.41	0.25	0.38	4.01	6.70	10.69	10.81	3.59	0.73	2.69	<1.6	HII	HII
12171-1156	4234	56.65	0.22	0.51	4.54	6.65	8.85	10.63	2.37	0.20	3.08	<1.9	HII	HII
12286-2600	5970	80.00	0.17	0.59	3.95	6.49	6.73	10.89	4.29	0.51	2.93	<1.4	HII	HII
12329-3938	3523	47.11	0.46	1.39	4.31	5.40	3.10	10.56	1.47	0.47	2.50	1.6	Sy2	Sy2

TABLE 4—Continued

Name (1)	Vel. (2)	D (3)	S_{12} (4)	S_{25} (5)	S_{60} (6)	S_{100} (7)	$\frac{S_{60}}{S_{25}}$ (8)	$\text{Log}(\frac{L_{IR}}{L_{\odot}})$ (9)	P_{FIR} (10)	$P_{4.8}$ (11)	q (12)	S_{LBA} (13)	V95 Class (14)	K01 Class (15)
12351-4015	5250	70.31	0.45	0.84	7.11	16.00	8.47	11.09	6.82	0.95	2.86	<2.0	HII/AMB/AMB	HII/HII/AMB
12596-1529	4773	63.89	0.34	1.36	7.38	9.09	5.43	10.95	4.61	0.60	2.88	<1.6	HII/HII/HII	HII/HII/HII
13001-2339	6446	86.41	0.14	0.85	13.70	15.30	16.19	11.37	15.20	3.28	2.67	<1.4	L	AMB
13035-4008	4475	59.89	0.68	1.22	5.66	8.79	4.64	10.89	3.37	0.54	2.79	<1.3	Sy1	Sy1
13097-1531	6400	85.79	0.34	0.96	11.10	20.90	11.51	11.38	14.65	2.58	2.75	2.5	B	HII
13135-2801	4426	59.23	0.18	0.71	4.72	8.91	6.63	10.72	2.97	0.37	2.91	2.2	HII	HII
13193-5208	5090	68.15	0.20	0.67	4.41	6.05	6.54	10.78	3.25	0.28	3.06	<2.0	HII	HII
13197-1627	5152	68.99	0.88	2.86	5.89	5.48	2.06	11.09	3.95	5.57	1.85	8.9	Sy1.8	Sy1.8
13229-2934	4112	55.01	0.64	2.40	16.90	28.60	7.04	11.19	8.78	2.50	2.55	<1.5	Sy2	Sy2
14544-4255	4875	65.26	0.35	1.31	7.61	12.80	5.81	11.01	5.55	2.19	2.40	3.8	Sy2	Sy2
14566-1629	3521	47.08	0.19	0.59	6.21	8.96	10.49	10.57	2.23	11.81	1.28	266.1	Sy2	Sy2
15555-6610	3638	48.65	0.21	0.30	2.41	12.40	8.09	10.48	1.77	ND	...	<1.5	Sy2	Sy2
16153-7001	3542	47.37	0.48	0.68	6.85	17.90	10.07	10.75	3.21	0.37	2.93	<1.3	N	N
16229-6640	6535	87.61	0.19	0.50	4.42	8.99	8.86	11.03	6.29	0.90	2.84	<1.4	AMB/HII	HII/HII
17138-1017	5261	70.45	0.62	2.07	15.20	19.00	7.34	11.33	11.61	1.51	2.89	<1.5	HII	HII
17182-7353	4788	64.10	0.16	0.27	3.58	9.30	13.16	10.70	3.06	0.60	2.71	<1.7	N	N
17260-7622	5507	73.76	0.17	0.43	4.07	5.36	9.38	10.79	3.47	0.91	2.58	<1.6	HII	HII
18093-5744	5200	69.63	0.65	2.38	15.20	25.10	6.39	11.36	12.53	1.81	2.84	<1.4	HII	HII
18293-3413	5449	72.98	1.12	3.76	34.20	49.70	9.10	11.71	29.52	5.06	2.77	<2.1	N	N
18341-5732	4601	61.58	0.37	1.27	14.40	25.20	11.34	11.19	9.50	1.08	2.94	<1.8	AMB	HII
18421-5049	5266	70.52	0.15	0.52	5.27	7.97	10.21	10.86	4.31	0.58	2.87	<1.5	B	HII
18429-6312	4367	58.44	0.23	0.76	4.38	8.15	5.75	10.70	2.67	0.32	2.92	<1.8	Sy2	Sy2
19543-3804	5713	76.54	0.37	1.17	6.05	9.14	5.17	11.06	5.83	4.32	2.13	23.4	Sy2	Sy2
20305-0211	5970	80.00	0.36	0.51	5.59	14.30	10.92	11.11	7.39	3.01	2.39	<1.7	HII/HII	HII/HII
20309-1132	3549	47.46	0.22	0.45	4.30	7.31	9.56	10.47	1.67	0.24	2.84	<1.7	HII	HII
20486-4857	5288	70.82	0.31	0.44	4.51	9.04	10.20	10.88	4.17	0.66	2.80	<1.7	N	N
21008-4347	5208	69.74	0.29	0.78	6.93	12.60	8.94	11.01	5.96	0.88	2.83	<1.7	HII	HII
21314-4102	5161	69.11	0.26	0.46	3.95	9.25	8.55	10.83	3.73	0.46	2.91	<1.4	L	AMB
21330-3846	5714	76.55	0.28	0.88	5.86	8.91	6.66	11.02	5.66	0.72	2.90	<1.7	L/HII	HII/HII
21453-3511	4842	64.82	0.59	2.12	16.50	25.60	7.78	11.31	11.51	3.25	2.55	4.7	Sy2	Sy2
22115-3013	4291	57.42	0.15	0.84	4.15	4.34	4.96	10.59	1.99	0.28	2.85	<1.7	HII	HII
22118-2742	5247	70.27	0.41	0.58	5.46	12.10	9.41	10.98	5.20	0.96	2.73	<2.6	HII	HII
22179-2455	4688	62.75	0.24	0.43	3.97	7.02	9.19	10.69	2.73	0.44	2.79	<2.5	N	N
23394-0353	6966	93.42	0.98	0.45	0.69	1.61	1.55	10.96	1.19	1.82	1.82	<1.5	HII	HII

Note. — The 12, 25, 60, 100 μm fluxes are taken from the *IRAS Faint Source Catalogue*. The ATCA 4.8GHz total radio power ($P_{4.8}$) and the high resolution LBA flux (S_{LBA}) of the galaxies are taken from Paper I. P_{FIR} is the FIR power of the galaxies. For a source with flux S_{ν} at a given frequency ν the power P_{ν} is defined as $4\pi D_L S_{\nu}$. q is defined as $\text{Log}(P_{FIR}/P_{4.8})$. Units are as follows: (2) km s^{-1} , (3) Mpc, (4-7) Jy, (10) $\times 10^{24} \text{ W Hz}^{-1}$ (11) $\times 10^{21} \text{ W Hz}^{-1}$ (13) mJy

TABLE 5

TABLE SUMMARIZING THE DISTRIBUTION OF GALAXY SPECTRAL CLASSIFICATIONS (BASED ON THE K01 SYSTEM) WITH LUMINOSITY. THE DISTRIBUTION FOR GALAXIES CLASSIFIED WITH THE V95 SYSTEM IS SHOWN IN BRACKETS.

$\log(L_{\text{IR}}/L_{\odot})$	HII	Sy	LINERs	Borderline	Ambiguous	Not classified
< 10.75	13 (13)	4 (4)	0 (0)	0 (0)	0 (0)	5 (5)
10.75-11.00	26 (20)	3 (3)	0 (2)	2 (5)	1 (2)	8 (8)
11.00-11.25	14 (7)	4 (4)	0 (2)	0 (2)	1 (4)	1 (1)
> 11.25	7 (5)	1 (1)	0 (2)	0 (1)	2 (1)	1 (1)

TABLE 6

TABLE SHOWING THE MEAN, MEDIAN AND STANDARD DEVIATION OF THE VALUE q FOR THE COLA SAMPLE AS A FUNCTION OF THE (K01) SPECTRAL CLASSIFICATION.

Galaxy spectral type	No.	Mean q	Median q	σ
All galaxies	90	2.76	2.80	0.27
All Seyferts	11	2.54	2.41	0.48
<i>Sy w. cores</i>	6	2.12	2.27	0.49
<i>Sy w/o cores</i>	5	2.75	2.79	0.16
All HII	59	2.81	2.83	0.20
<i>HII w. cores</i>	3	2.75	2.75	0.15
<i>HII w/o cores</i>	55 ¹	2.81	2.84	0.21
Ambiguous	4	2.79	2.78	0.11
Borderline	2	2.83	2.83	0.07
Not classified	15	2.77	2.79	0.12

Note. — ¹ One starburst galaxy (IRAS 05035-0805) was not observed with the LBA and is therefore excluded from the sample of HII galaxies without cores.

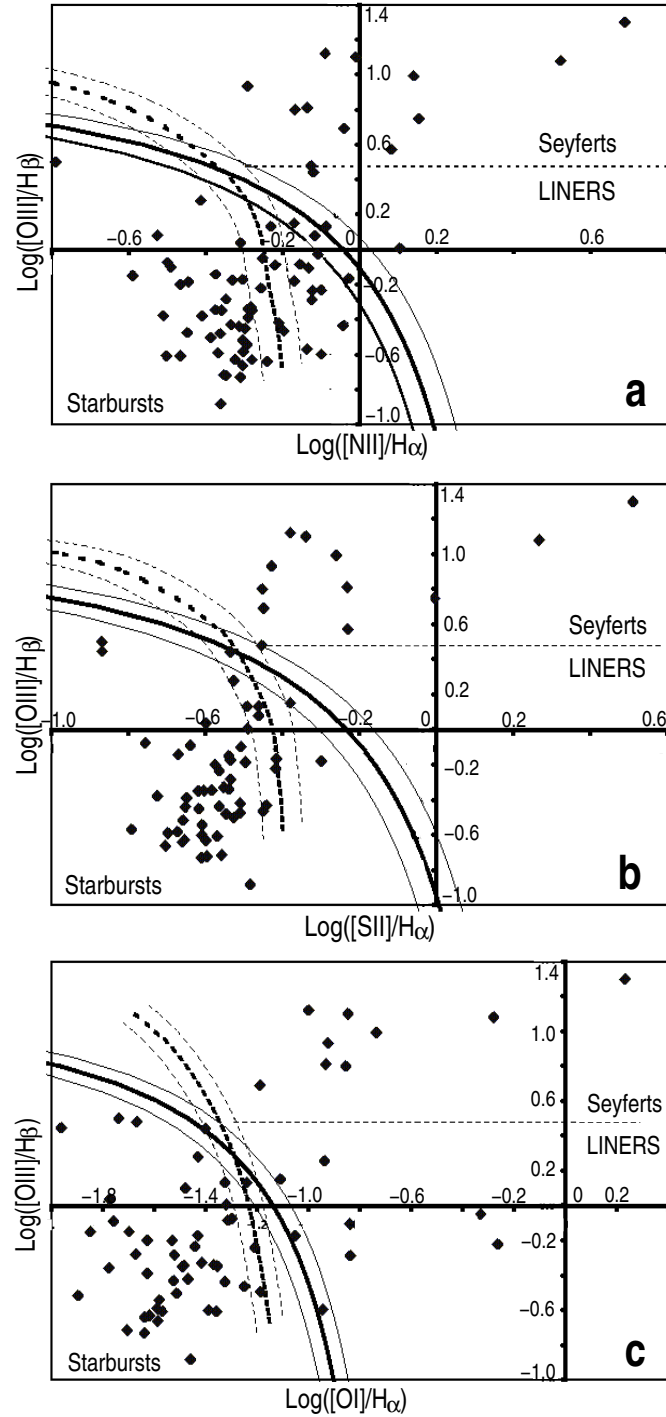


FIG. 1.— Diagnostic diagrams for emission line ratios. The dotted lines indicate the HII/AGN partition ($\pm 0.5\text{dex}$) for the V95 classification system and the solid lines show the theoretical HII/AGN partition ($\pm 0.5\text{dex}$) from the K01 system.

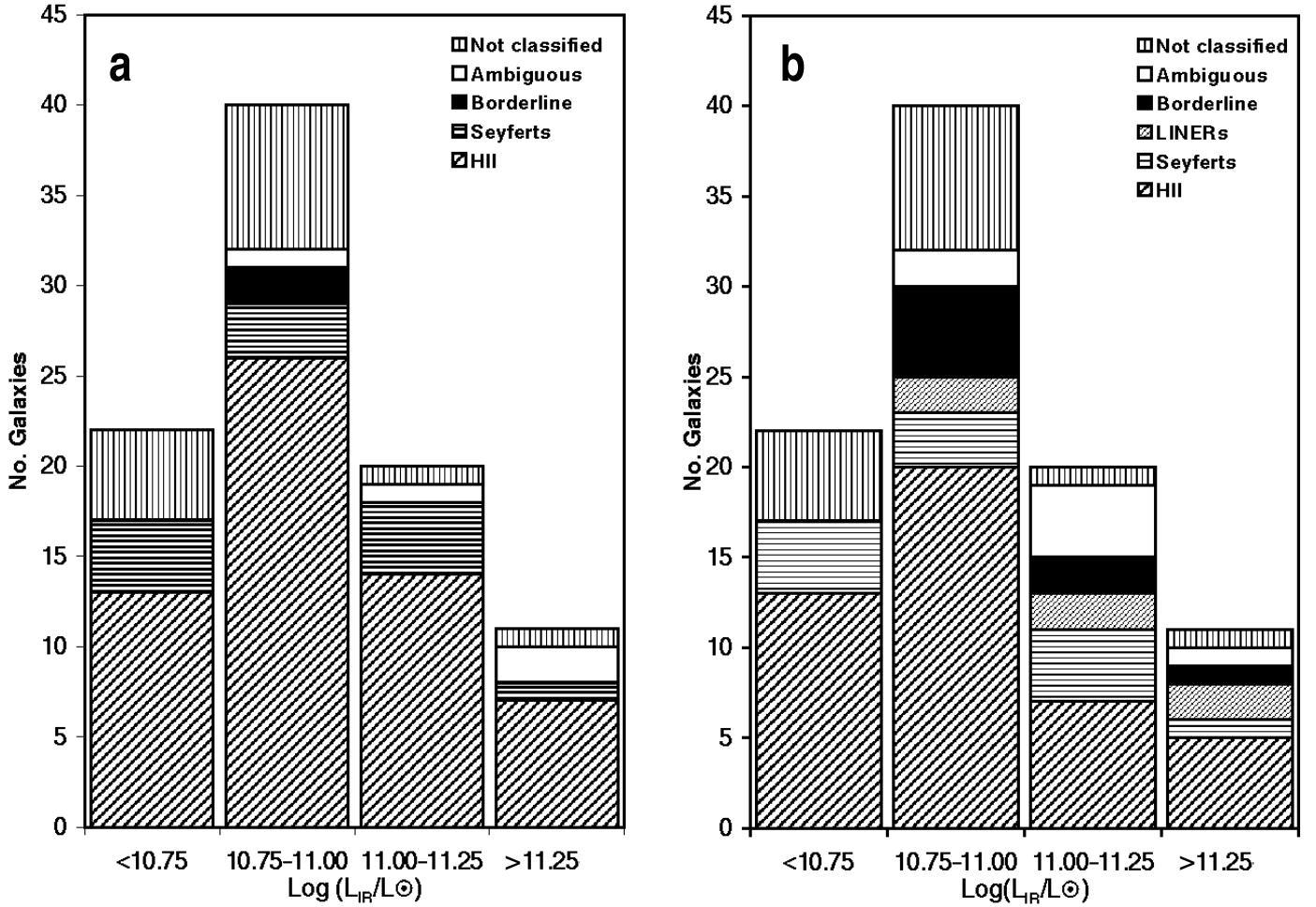


FIG. 2.— a) The distribution of the classification of the galaxies of our sample as a function of L_{IR} using the K01 scheme. b) Same as in a) but using the V95 scheme. Note that even though no significant trend with luminosity was seen in the Seyferts, the proportion of LINERS, borderline and ambiguous galaxies rises when one uses the V95 system.

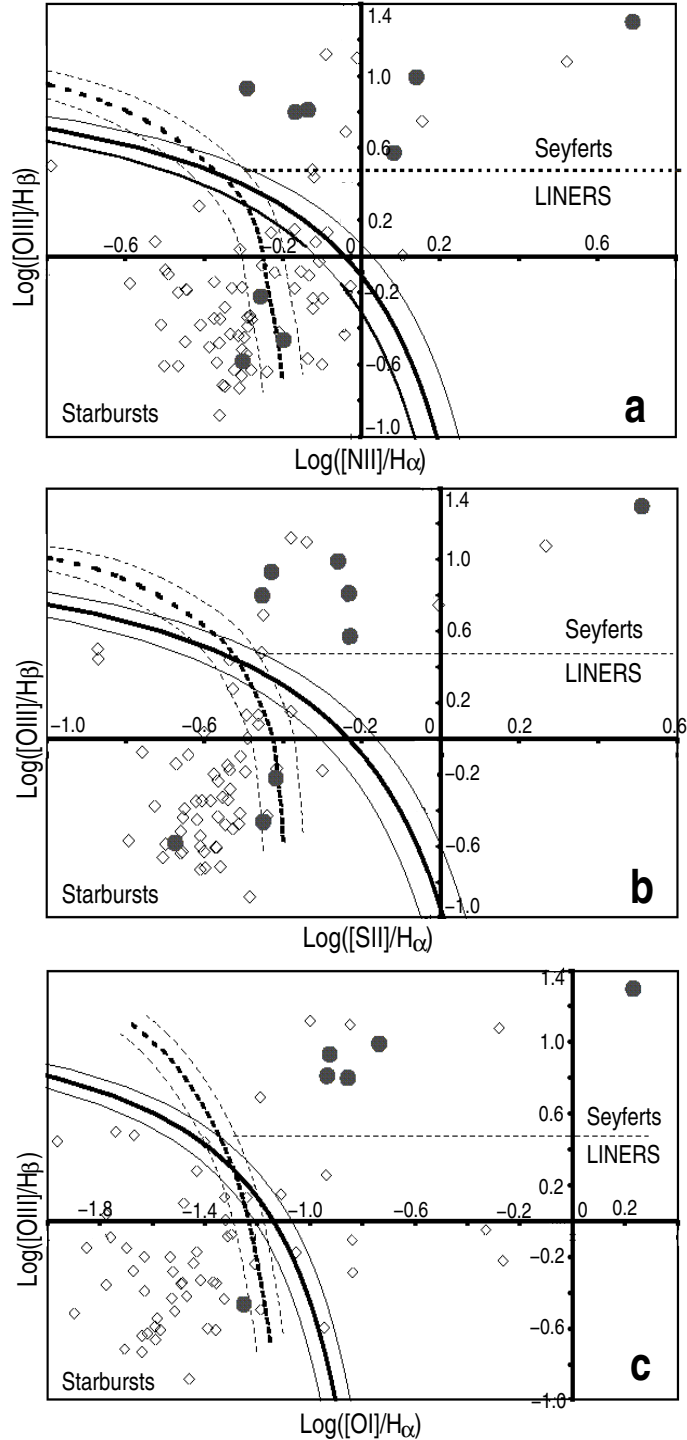


FIG. 3.— The same diagnostic diagrams presented in Fig. 1 with the galaxies in which compact radio cores were detected marked with filled symbols.

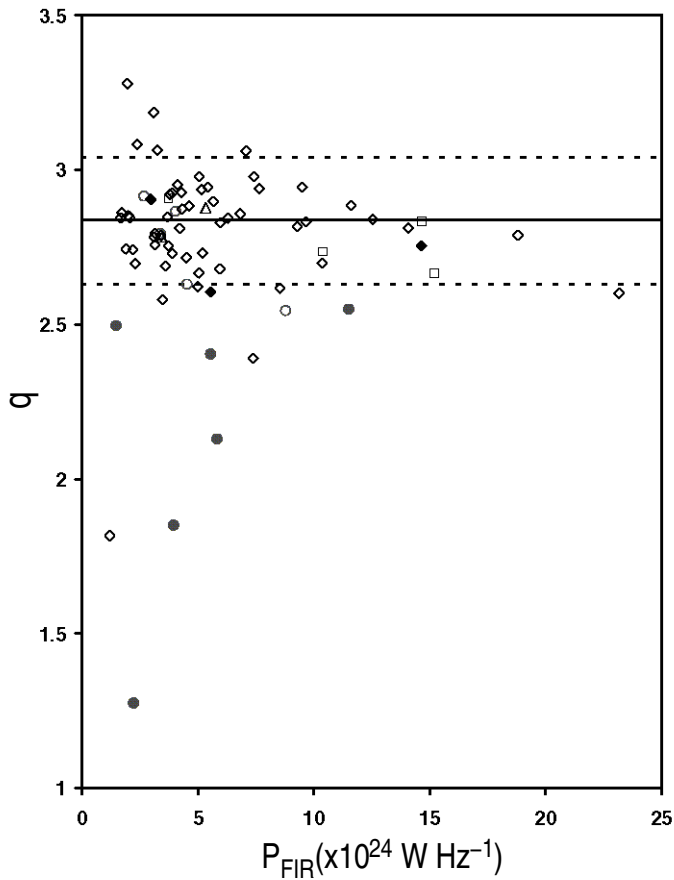


FIG. 4.— Plot of q versus the galaxy FIR power. Galaxies classified as starburst galaxies are represented by diamonds, Seyferts by circles, borderline galaxies by triangles and ambiguous classifications by squares. Filled symbols indicate those galaxies in which a compact radio core were detected. A solid line indicates is shown at $q=2.84$, the median q for the starburst galaxies without cores, with dotted lines at $\pm 1\sigma$.

APPENDIX

NOTES ON INDIVIDUAL GALAXIES

Seyfert galaxies in which compact radio cores were detected

- **12329-3938 (NGC 4507)** (Sy2; $q=2.5$) is a barred spiral galaxy (SAB(s)ab; Sandage & Brucato 1979). It is a known Sy2 galaxy (de Grijp et al. 1987; Vaceli et al. 1997). A tentative detection of a $< 0.05''$ core at 1.6 mJy ($10^{3.4} L_\odot$) was reported in Paper I, making this source the lowest luminosity core detection in the sample.
- **IRAS 13197-1627** (Sy1.8; $q=1.85$) is a known Seyfert galaxy (de Grijp et al. 1985) and is classified as a Seyfert 1.8 by Aguero et al. (1994). The narrow emission lines in this object are unusually broad (FWHM of [OIII] $\lambda 5007 \sim 1000 \text{ km s}^{-1}$, FWHM of [NII] $\lambda 5007 \sim 700 \text{ km s}^{-1}$) but symmetrical. Evidence of a broad H α line is seen in our spectra but the H β line has a similar width to the [OIII] lines. It has a tentative morphological classification in the *NASA Extra-galactic Database* (NED) as a barred spiral galaxy. A compact ($< 0.05''$) core of 8.9 mJy was reported in Paper I and VLA observations at 4.8GHz by Kinney et al. (2000) have revealed a linear structure extending about 278pc from the core, believed to be a synchrotron jet. IRAS 13197-1627 exhibits one of the lowest values of q in our sample. This radio excess remains after subtraction of the compact core emission and is probably due, at least in part, to emission from the ~ 300 pc-scale radio jet.
- **IRAS 14544-4255 (IC4518A)** (Sy2; $q=2.4$) is one of a pair of strongly interacting galaxies (Condon et al. 1996) and has not been previously identified as a Seyfert galaxy. This source exhibits a large radio excess and the 3.77 mJy ($10^{4.1} L_\odot$) compact radio core (Paper I) contributes only 3.5% of the total radio emission.
- **IRAS 14566-1629 (NGC 5793)** (Sy2; $q=1.28$) has an Sb classification (NED) and is one of a pair of galaxies. VLBI observations of this source have detected a compact nucleus ($0.016''$) which is extended parallel to the minor axis of the galaxy (Gardner 1992). There is also some evidence for a water maser with a diameter larger than 20pc (Hagiwara et al. 1997). It is a known Seyfert 2 (Baan et al. 1998) and exhibits both the largest radio excess and the brightest radio core ($10^{5.6} L_\odot$) of the galaxies in our sample (Paper I), accounting for 30% of the observed radio flux. This source exhibits the coolest FIR colours of the Seyferts in our sample ($S_{60}/S_{25}=10.5$) presumably indicating that star formation dominates the IR spectrum but not at optical or radio wavelengths.
- **IRAS 19543-3804** (Sy2; $q=2.13$) is classified as a spiral galaxy (Sb or IrS) in a cluster. A compact ($< 0.05''$) core was detected with a flux of 23.4 mJy ($10^{4.9} L_\odot$; Paper I). This core is one of the brightest we detect and accounts for 32% of the total radio luminosity at 2.3 GHz. This source exhibits a large radio excess and subtraction of the compact core reduces the radio excess to $\sim 40\%$.
- **IRAS 21453-3511 (NGC7130, IC5135)** (Sy2; $q=2.55$) is a known AGN, identified by Phillips et al. (1983) as a Seyfert 2 active nucleus surrounded by a starburst ring. Observations by Thuan (1984) further showed that the starburst dominates the galaxy emission, contributing 75% of the emission in the UV. Its optical emission line ratios have confirmed its AGN classification but it falls on the borderline between the Sy2 and LINER classes with Veilleux et al. (1995) classifying it as a LINER while both Heisler et al. (1997) and Vaceli et al. (1997) classify it as a Seyfert 2. We also classify it as a Seyfert 2 and it is possible that the differences between the classifications reflect differing contributions from the starburst emission in the slit.

A 4.7 mJy ($10^{4.1} L_\odot$) core was detected in IRAS 21453-3511 (Paper I) and the 4.8 GHz luminosity of the galaxy is nearly twice that predicted from the FIR luminosity. Heisler et al. (1997) measured a compact core flux at 2.3 GHz of 14 mJy using the PTI baseline with a resolution of $0.1''$, twice that of ours, which implies that the source has compact radio structures between 25-50pc in size which we have resolved out. These structures could be associated with a radio jet. Alternatively, the difference between the PTI flux and our measurements could be due to intrinsic variability of the compact core.

Seyfert galaxies in which compact cores were not detected

- **IRAS 03022-1232 (NGC 1204)** (Sy2; $q=2.87$) was classified as a LINER galaxy by V95 with $\log(\text{OIII}/\text{H}\beta)=0.47$. We measure $\log(\text{OIII}/\text{H}\beta)=0.48$ classifying it as a Sy2, but in any case it clearly lies on the border between the LINER and Seyfert classes in the V95 system. It has an SO/a morphology (NED). No compact radio core was detected ($< 1.8 \text{ mJy}$; Paper I), indicating that any radio core must have a luminosity $< 10^{3.6} L_\odot$. This source does not exhibit a radio excess indicating that the radio continuum is probably dominated by star formation.
- **IRAS 04461-0624 (NGC1667)** (Sy2; $q=2.63$) is a known Seyfert galaxy (Phillips et al. 1983). Although it appears that H α is slightly broadened in our spectrum, we find that both the [NII] emission lines are broadened in a similar fashion (this was also seen by Ho et al. (1997a)) and we therefore conclude that no broad emission line component is visible. Spectropolarimetric observations of this source (Tran et al. 2001) have not revealed a hidden broad line region in this object. Thean et al. (2000) measure a compact core ($< 0.3''$) with a 4.8GHz flux of 1.5 mJy but we detected no compact radio ($< 0.05''$) core ($< 1.6 \text{ mJy}$; Paper I) indicating that any radio core must have a luminosity $< 10^{3.7} L_\odot$. Since one would expect it to be brighter at 2.3GHz than at 4.8GHz (assuming

a spectral index of 0.7), our non-detection of a core implies that the core is either larger than $< 0.05''$ and hence much of the flux is resolved out or has a flat spectral index. This source is one of the two Seyfert galaxies with cool FIR colours ($S_{60}/S_{25}=8.8$)

- **IRAS 13035-4008 (ESO 323-G77)** (Sy1; $q=2.79$) is a known Seyfert 1 galaxy (Fairall 1986) and is classified in NED as a barred spiral galaxy. Broad emission lines are clearly visible in both $H\alpha$ and $H\beta$. No compact radio core was detected (< 1.3 mJy; Paper I) indicating that any radio core must have a luminosity $< 10^{3.5}L_\odot$. This source does not exhibit a radio excess indicating that the radio continuum is probably dominated by star formation.
- **IRAS 13229-2934 (NGC5135)** (Sy2; $q=2.55$) is a known Sy2 galaxy (Phillips et al. 1983) and has barred spiral morphology (NED). No compact radio ($< 0.05''$) core was detected (< 1.5 mJy; Paper I) indicating that any radio core must have a luminosity $< 10^{3.5}L_\odot$. This source was also observed by Thean et al. (2000) who failed to detect compact radio emission from the nucleus. IRAS 13229-2934 does exhibit a similar radio excess to IRAS 21453-3511 which may be due to the extended structure and radio lobes detected by Bransford et al (1998) and Thean et al. (2000).
- **IRAS 18429-6312** (Sy2; $q=2.92$) is a known Sy2 galaxy (Fairall 1979) and has an SB morphology (NED). No compact radio core was detected (< 1.8 mJy) indicating that any radio core must have a luminosity $< 10^{3.7}L_\odot$. This source exhibits a radio *deficit* indicating that the radio continuum is dominated by star formation.

Non-Seyfert galaxies in which compact cores were detected

- **IRAS 09375-6951** (HII; $q=2.61$) is classified in the NASA Extragalactic Database (NED) as an irregular spiral galaxy. We classify this object as a starburst using the K01 scheme and a borderline or composite object (e.g. Hill et al. 1999; Barth & Shields 2000). A compact ($< 0.05''$) core was detected with a flux of 3.6 mJy ($10^{4.25}L_\odot$; Paper I) which contributes 13% of the total radio emission. IRAS 09375-6951 could either contain an AGN which is obscured at optical wavelengths or a complex of supernovae remnants (e.g. Arp220; Smith et al. 1998b). As discussed in Section 2.2.2, Kewley et al. (2000) found that the sources they believed to be complexes of SNR tended to have compact cores with luminosities of $< 10^4L_\odot$. The $0.05''$ compact core in IRAS 09375-6951 has a luminosity which would place it among the AGN rather than the starburst galaxies.
- **IRAS 13135-2801 (NGC 5051)** (HII; $q=2.91$) is an SA(rs)b galaxy with a nuclear ring (Buta 1995). We detect a compact core in both polarizations at the level of 2.2 mJy ($10^{3.75}L_\odot$). This is the only object with a compact radio core which exhibits a *deficit* in radio flux, emitting 17% *less* radio flux than would be predicted from the FIR luminosity. The optical line ratios exhibited by this galaxy place it in the starburst of HII regime. The low luminosity of the radio core combined with the optical spectroscopic classification means that it is highly possible that we have detected a complex of radio supernovae in this object rather than an AGN.
- **IRAS 13097-1531 (NGC 1510)** (HII; $q=2.75$) is an S0 (or peculiar spiral) and is known to contain an OH megamaser (Martin et al. 1989). It has been classified from optical spectra as a “composite object” by Baan et al. (1998) (who used a similar classification system to V95) and our own observations show that it lies close to the AGN/HII region partition in the V95 classification system. Under the K01 classification system it is classified as a starburst (HII) galaxy. A compact radio core at the level of 2.5 mJy was detected (Paper I). IRAS 13097-1531 is similar to IRAS 09375-6951 in that the optical classification is ambiguous but the radio luminosity of the core is $10^{4.14}L_\odot$, brighter than would be expected for the supernova complexes.